A GLOBAL SENSITIVITY ANALYSIS OF SOLAR VIRUS INACTIVATION MODELING

BY

XINYI ZHANG

THESIS

Submitted in partial fulfillment of the requirements
for the degree of Master of Science in Environmental Engineering in Civil Engineering
in the Graduate College of the
University of Illinois at Urbana-Champaign, 2019

Urbana, Illinois

Adviser:

Assistant Professor Jeremy S. Guest

ABSTRACT

Waterborne pathogens related to the lack of safe drinking water and surface water contamination pose a substantial threat to human health. Sunlight-mediated inactivation of waterborne pathogens has been widely studied in natural surface waters, and it has been leveraged as a low-cost approach to disinfection for drinking water and wastewater treatment. Solar-driven disinfection systems can inactivate virus in water through two major mechanisms: direct endogenous mechanism causes damage to viral components (e.g. DNA/RNA, proteins) upon their absorption of sunlight photons (mostly UVB); indirect exogenous inactivation refers to the viral component damage caused by reactive intermediates, whose production is sensitized by external chromophores upon their absorption of sunlight photons (UVA and visible light). The solar virus inactivation process is affected by a wide range of factors, including sunlight irradiance, water absorbance, concentrations of photosensitizers, and water depth, among others.

To elucidate the relative importance of environmental, water quality, photo-reactivity and engineering design parameters in solar virus inactivation in treatment systems, this study adapted and combined the aqueous photochemistry model, APEX, with the sunlight irradiance modeling program, SMARTS, to include different independent factors in a mathematical framework. The uncertainty of each parameter was characterized and incorporated into the Monte Carlo simulation of the integrated mechanistic model for three virus species (MS2 bacteriophage, phiX174 bacteriophage, and human adenovirus) and two water types (natural surface water, waste stabilization pond water), and a global sensitivity analysis was performed to quantitatively apportion the uncertainty of solar virus inactivation rate constant to different sources.

This work demonstrated that environmental (location, diurnal and seasonal motion of the sun) and engineering design parameters (water depth) significantly outweigh water quality and photo-reactivity parameters in the determination of virus inactivation rate constants. System reliability and efficiency of a solar-driven disinfection system can be improved by optimizing its geometry configuration for sunlight exposure. Further Monte Carlo simulation of a 3D continuous stirred-tank reactor model coupled with the integrated solar virus inactivation model was performed to investigate the effect of different designs on the virus removal rate of a maturation pond system. Results showed that increasing the hydraulic retention time and the

hydraulic efficiency are more cost-effective strategies than reducing pond depth for the improvement of virus removal. The analysis also revealed the trade-off between the solar virus removal performance and the diurnal fluctuation of effluent quality.

ACKNOWLEDGEMENTS

I would like to first express profound gratitude to my advisor Dr. Jeremy S. Guest for all the support and guidance he has provided throughout the completion of my research project. His insight and dedication to quantitative sustainable design have greatly inspired me and motivated me to commit to this field.

I would also like to thank my colleagues in Guest Research Group for the help and encouragement in the past two years. It has been a pleasure to work with such a dynamic and loving group of people. I am grateful for the valuable input to this research project from our previous group member, Amanda Lardizabal.

I appreciate the valuable advice from our collaborators, particularly Dr. Andrea I. Silverman at New York University, Dr. Davide Vione at University of Turin, and Dr. Thanh H. Nguyen at University of Illinois at Urbana-Champaign.

Special acknowledgements also go to my family for their unconditional love, and to Daniel for bringing so much joy and fun to my life.

TABLE OF CONTENTS

CHAPTER 1: INTRODUCTION

Waterborne pathogens pose a substantial threat to human health worldwide. It is estimated that waterborne diseases that are closely related to unsafe drinking water, unsafe sanitation and lack of hygiene have caused 870,000 deaths in 2016 (World Health Organization, 2018). For example, rotavirus, which features low infectious dose and long survival in surface water, accounted for 197,000 – 233,000 child deaths globally in 2013 (World Health Organization, 2016). Safely managed drinking-water services were still unavailable to 29% of global population in 2015, whereas the population having access to safely managed sanitation services barely made up 39% (World Health Organization, 2018). As a result, the Sustainable Development Goals include multiple targets regarding reduction of deaths and illness from water contamination as well as ensuring universal access to safe and affordable water and sanitation (United Nations, 2015).

Sunlight is known to be a pertinent contributor to the inactivation of viral and bacterial pathogens in the aquatic environment. It is responsible for reducing concentrations of pathogens in natural recreational waters and helps control the health risks for bathers (World Health Organization, 2000). Leveraging the sunlight energy is a common strategy in low-cost water and wastewater treatment technologies. Waste stabilization ponds (WSPs) and constructed wetland are two examples of engineered wastewater treatment systems utilizing sunlight-mediated disinfection (Victor et al., 2006). Effluents of these systems can potentially be reused for agricultural irrigation with the benefit of nutrient recovery (Verbyla and Mihelcic, 2015a). Solar disinfection of drinking water (SODIS) has also gained popularity as a low-cost household water treatment technology in developing countries where full-scale water management infrastructure is still absent (McGuigan et al., 2012). The most distinguished advantages commonly shared by these technologies are low costs of construction, operation and maintenance as well as less concern regarding disinfection byproducts. It is commented by Verbyla et al. (2017) that full-scale WSP systems can have up to 6-log removal of fecal bacteria and 4-log removal of viruses. Despite the advantages and the promising disinfection potential, the efficiency of pathogen removal of treatment systems using solar-driven inactivation is highly variable and mostly not optimal (Liu et al., 2016). Identifying the sources of uncertainty of pathogen removal efficiency

and understanding their relative contributions are critical for improving the designs and increasing the reliability of the engineered treatment systems.

In the past decades, tremendous progress has been made in identifying the factors affecting pathogen removal of solar-driven treatment systems. Early efforts have been focused on common indicators of the physicochemical conditions of water (e.g., temperature, pH, turbidity and dissolved oxygen (DO)) and design parameters that either directly affect sunlight-mediated inactivation (water depth) or generally influence the hydraulic efficiency of the reactor (including length-to-width ratio, inlet/outlet settings, baffle configurations etc.). Most of these studies relied on field monitoring of a few number of systems and simplified modeling. More complicated hydrodynamic models involving environmental factors, such as wind speed and sunlight exposure, were developed to simulate pathogen removal efficiency of a system. However, a common defect of these models is that the sunlight inactivation process of pathogens was simplified into a first-order kinetic reaction, whose rate constant is derived from a non-linear regression model involving temperature, pH, turbidity and DO. The mechanisms of sunlight inactivation of pathogens are not well understood or incorporated into the models.

Fortunately, great progress in the mechanistic understanding of sunlight inactivation processes in the past years has provided opportunities of more sophisticated and accurate modeling. Waterborne viruses, having the simplest structures among waterborne microorganisms, can be inactivated by natural sunlight through two major mechanisms (Nelson et al., 2018): 1) direct endogenous inactivation is caused by direct absorption of sunlight (mostly UVB) photons by viral components; 2) exogenous inactivation refers to the viral component damage caused by photo-produced reactive intermediates (PPRIs), such as reactive oxygen species (ROS), which are produced from photosensitizers in water upon their absorption of sunlight photons. It implies that the virus removal of a treatment system is composed of multiple steps: 1) sunlight irradiation on water surface; 2) sunlight penetration and absorption in the water body; 3) direct damage and/or photooxidation of viral components. Each step is affected by a wide range of factors. Sunlight spectrum incident on water surface is determined by a series of environmental factors, including location, elevation, diurnal and seasonal shifts, meteorological and atmospheric conditions etc. The transmission and absorption of incident sunlight depend on the water constituents (such as the concentration of colored dissolved organic matter (CDOM),

and turbidity) and the optical path, which is affected by the zenith angle of incident sunlight, the refraction at the air-water interface, and the depth of the water body. The composition of the virus (e.g. DNA/RNA, proteins) has a great influence on its susceptibility to direct sunlight inactivation. The water physicochemical conditions, including concentrations of photosensitizers, pH, DO etc., on the other hand, affect the viral exposure to PPRIs and consequentially the exogenous inactivation. Additionally, just like any other reactions, the efficiency of virus removal is subject to the influences of design and operation of the treatment system.

Although recent studies have revealed that the abovementioned factors have different and complicated influences on the sunlight-mediated virus inactivation, the interactive and interrelated effects of these factors are yet investigated sufficiently (Li et al., 2018). To understand the sources of uncertainty in solar virus inactivation without losing information of the interactions among different factors, uncertainties of the factors should be included and investigated simultaneously in modelling or experiment. Given the limited combinations of experimental conditions, it is more systematic and efficient to examine the effects of multiple factors using modelling and statistical methods.

The objective of this study is to elucidate the relative importance of various environmental, photo-reactivity, water quality and engineering design parameters for solar virus inactivation by leveraging mechanistic modeling and global sensitivity analysis methods. For this purpose, a global sensitivity analysis was performed by integrating models that characterize the sunlight irradiance incident on water surface and the inactivation chemistry in water body. Two models were adapted and integrated: 1) the sunlight irradiance modeling program SMARTS (Simple Model of the Atmospheric Radiative Transfer of Sunshine) (Gueymard, 1995), and 2) the aqueous photochemistry model APEX (Aqueous Photochemistry of Environmentally occurring Xenobiotics) (Bodrato and Vione, 2014). The uncertainties of 15 environmental, photo-reactivity, water quality and engineering design parameters in the integrated model were characterized based on existing knowledge and global datasets. Monte Carlo simulations were run across the multivariant distribution of the parameters for bacteriophage MS2, phiX174 and adenovirus in natural surface water and in WSP water. The simulation output, total inactivation rate constant, was used to estimate sensitivity indices in Morris One-at-A-Time screening

method and subsequently Sobol variance-based sensitivity indices. Finally, the log removal of MS2 of a maturation pond of different designs was predicted using a simplified continuous stirred-tank reactor (CSTR) model coupled with the integrated solar virus inactivation model to illustrate the influence of pond design on its virus inactivation performance.

The rest of this thesis is organized as follows:

- Chapter 2 provides background including existing knowledge of solar virus inactivation mechanisms and its application as well as a comparative review of global sensitivity analysis methods.
- Chapter 3 presents the methods, results and discussion of the global sensitivity analysis of the integrated solar virus inactivation model.
- Chapter 4 summarizes the conclusions of the study and highlights its engineering significance.

CHAPTER 2: BACKGROUND

2.1 Overview of solar virus inactivation and its application

Sunlight exposure is the most important factor for the removal of viral and bacterial pathogens in engineered low-rate treatment systems for wastewater and stormwater, such as WSPs, wastewater storage and treatment reservoirs, and constructed wetlands (Dias et al., 2017; Silverman et al., 2015; Victor et al., 2006). WSP is the most widely used treatment system for disinfection in developing countries from Latin America (Noyola et al., 2012). It is also popular in developed countries, such as France, Germany, Australia and the US, especially in smaller towns and rural settings where large areas of open land are available (Li et al., 2018; Verbyla et al., 2017). Facultative ponds and maturation ponds are usually designed mainly for the objective of pathogen removal (Kayombo et al., 2005).

Several studies have reviewed and compared the main pathogen-removal mechanisms of WSP systems (Davies-Colley, 2005; Dias et al., 2017; Verbyla et al., 2017; Verbyla and Mihelcic, 2015a). For waterborne pathogens (bacteria, viruses, protozoan parasites and helminth eggs) in general, the removal mechanisms in WSP systems can be categorized into three groups: 1) solar-driven disinfection; 2) physical removal through attachment and sedimentation; and 3) "natural biological disinfection" through predation, starvation and competition.

Particularly, sunlight drives pathogen disinfection through various routes. Firstly, sunlight photons can directly damage pathogen components and can sensitize the production of damaging reactive species in cell or in bulk water, which together will be referred to as solar inactivation hereafter. Diurnal and seasonal solar motions affect water temperature, and high temperature can increase the die-off rate of pathogens by exerting a thermal shock, albeit insignificant below 45°C (Carratalà et al., 2016; Davies-Colley, 2005; Maiga et al., 2009). High temperature also accelerates the diffusion of water constituents (e.g. PPRIs, photosensitizers, predators, and algae toxins) and, as a result, facilitates exogenous solar inactivation. This positive correlation between solar inactivation rate and temperature are significant when other essential conditions for exogenous inactivation are met (Romero et al., 2011). Additionally, sunlight irradiation provides energy for photosynthesis by algae or other microorganisms in water, which increases the DO concentration and raises the pH by consuming dissolved CO_2.

High pH in turn can cause damage to microbial components, but this effect is significant only when pH exceeds 9.0 (Dias et al., 2017). Apart from the direct damage caused by high pH, abundance of hydroxyl ion and DO can also facilitate the indirect solar inactivation by providing intermediates to produce pathogen-damaging reactive species.

Compared to other microorganisms, viruses have much smaller sizes and simpler structures. As a result, it is unlikely that viruses in WSPs can be efficiently removed through sedimentation, unless they are sorbed onto settleable solids, such as algae or wastewater solids (Davies-Colley, 2005). Studies on virus removal rate through sedimentation are rare. With regard to "natural disinfection", Davies-Colley (2005) commented that the removal of virus-like particles by flagellate ingestion is highly likely in WSPs at times and places of low sunlight exposure. Yet the quantification of this process is absent so far. On the other hand, since the reproduction and transmission of viruses are independent of nutrients or substrates in the environment, starvation or competition does not seem to play an important role for virus removal.

In general, solar inactivation is the single most important mechanism for virus disinfection in the abovementioned treatment systems. DO, pH, temperature and sunlight penetration, well recognized as the important factors for solar inactivation, are highly correlated in observations of full-scale treatment systems (Davies-Colley et al., 1999). Therefore, to understand the influence of individual factor on solar inactivation, it is critical to go beyond statistical modeling and gain mechanistic understandings of solar inactivation through physical experiments. Davies-Colley et al. (1999) summarized and verified the three major mechanisms of solar inactivation through controlled experiments and reasonable inference. Curtis et al. (1994) firstly characterized the penetration and attenuation of sunlight in WSPs, suggesting that CDOM in water has increasing absorption of longer wavelengths, while shorter wavelengths are more affected by algae and attenuate exponentially within a few centimeters of water (Dias and Von Sperling, 2017). Early efforts by Davies-Colley et al. (2000) showed that different virus species are inactivated by different components of the solar spectrum, which have differing dependencies on physicochemical conditions. Sinton et al. (2002) also observed that F-specific RNA bacteriophages were susceptible to a wide range of wavelengths, and the inactivation rate was DO-dependent, which suggested photooxidative damage. On the contrary, F-specific DNA

bacteriophages were inactivated mainly by shorter (UVB) wavelengths, which is consistent with photobiological damage. More studies examined the correlation between solar inactivation rate and various physicochemical (e.g. salinity, turbidity, NOM, or light-absorbing constituents) and environmental conditions, such as water depth (Bolton et al., 2010; Carratalà et al., 2016; Kohn et al., 2007; Kohn and Nelson, 2007; Maiga et al., 2009; Romero et al., 2011; Silverman et al., 2013; Sinton et al., 2002; Verbyla and Mihelcic, 2015a). These studies provided foundations and inspirations for more intricate studies into the mechanisms of solar inactivation.

2.2 Solar virus inactivation mechanisms and modeling

Three mechanisms have been identified for the solar inactivation of bacterial and viral pathogens in water: direct endogenous inactivation, indirect endogenous inactivation, and indirect exogenous inactivation (Nelson et al., 2018). Direct inactivation occurs when endogenous chromophores (e.g. nucleic acids, proteins, or other component macromolecules) are damaged upon their absorption of sunlight photons. Indirect inactivation refers to the damage caused by highly oxidizing reactive intermediates, the production of which is sensitized by chromophores when absorbing sunlight photons. Depending on the source of photosensitizers, indirect inactivation can either be endogenous or exogenous to the pathogen. Endogenous chromophores include RNA, DNA, proteins, NADH, etc. Both nucleic acids and amino acids have absorption of primarily photons in UVB range (280-320 nm). Other endogenous chromophores could also be able to absorb UVA (320-400 nm) and visible light (400-700 nm). Different virus species also exhibit various susceptibility to solar inactivation. MS2, due to its strong resistance to solar inactivation, is believed to be a conservative indicator and the first-choice surrogate for virus-removal efficiency (Amarasiri et al., 2017; Love et al., 2010; Verbyla and Mihelcic, 2015a). Consistent to previous findings, CDOM is the most important exogenous photosensitizer in water, absorbing a wide range of wavelengths, especially UVB. Apart from CDOM, nitrate, nitrite and metal complexes are also exogenous chromophores that can trigger indirect inactivation in natural water. Due to the relatively simple structures of viruses, there are few internal photosensitizers that can absorb wide range of sunlight, and thus, indirect endogenous inactivation tends to be insignificant compared to the other two mechanisms. As a result, most recent studies on solar virus inactivation focused on either direct endogenous mechanism or indirect exogenous mechanism.

2.2.1 Direct endogenous mechanism

Direct endogenous mechanism is found to contribute more or less to the inactivation of all viruses studied so far (Bosshard et al., 2013; Love et al., 2010; Mattle et al., 2015; Nguyen et al., 2014; Romero et al., 2011; Silverman et al., 2013). It is primarily attributed to UVB range sunlight. Depending on the structures of the nucleic acids and proteins, different virus species are likely to have different susceptibility to direct endogenous inactivation (Love et al., 2010). The direct endogenous inactivation was invariably modeled using pseudo first-order kinetics, since a linear correlation between the log removal and the reaction time was often observed (Fisher et al., 2011). The first-order inactivation rate constant k_{endo} is determined by the sunlight irradiance spectrum and the virus' relative susceptibility to different wavelengths on the spectrum. Different expressions of the k_{endo} have been proposed to model the direct endogenous mechanism. Fisher et al. (2011) and Silverman et al. (2019) modeled k_{endo} of a certain virus species using Equation (1).

$$k_{endo} = \int_0^\infty [I(\lambda) \times P(\lambda)]\, d\lambda \tag{1}$$

where $I(\lambda)$ is the spectral irradiance of sunlight (in $W \cdot m^{-2} \cdot nm^{-1}$), and $P(\lambda)$ is the spectral sensitivity coefficient (in $m^2 \cdot W^{-1} \cdot h^{-1}$), i.e., the relative contribution of photons at wavelength λ to the direct endogenous inactivation rate of the virus. $P(\lambda)$ is also known as the biological weighting function of the virus. The action spectra, $I(\lambda) \times P(\lambda)$, and the weighting function was estimated and calibrated for MS2 and PRD1 by Fisher et al. (2011) using empirical data. Silverman et al. (2019) updated the values of $P(\lambda)$ for MS2 with the latest knowledge of the effective wavelength range and different calibration methods. To account for light attenuation by water, the k_{endo} at a certain depth z is modeled similarly to Equation (1) but $I(\lambda)$ is substituted by the downward irradiance at the depth $E_d(z, \lambda)$, which can be estimated using Equation (2)~(4) for the wavelengths of interest (280-700 nm) (Nguyen et al., 2014).

$$E_d(z, \lambda) = E_d(0, \lambda) \cdot e^{-K_d(\lambda) z} \tag{2}$$

$$K_d(\lambda) \approx a(\lambda) \tag{3}$$

$$a(\lambda) = \frac{2.303\alpha(\lambda)}{l} \quad (4)$$

where $a(\lambda)$ (in m^{-1}) is the absorption coefficient of the water, and $\alpha(\lambda)$ is the measured decadic absorption coefficient with an optical length (l) equal to 1 cm. Fairly good agreement between the k_{endo} predicted by the action spectrum model and the measured k was observed by Nguyen et al. (2014). But they also pointed out that the model's ability to accurately predict the irradiance between 280-300nm was the major source of uncertainty.

Kohn et al. (2016) and Mattle et al. (2015) further decomposed the weighting function into a product of the extinction coefficient (i.e., molar absorption coefficient) $\varepsilon(\lambda)$ ($virus^{-1}\cdot cm^{-1}$) and the apparent quantum yield $\Phi(\lambda)$ ($virus \cdot photon^{-1} \cdot nm^{-1}$) or Φ ($virus \cdot photon^{-1}$), so that the modeling of direct endogenous inactivation is in a consistent manner with the modeling of direct photolysis of chemicals in APEX (Bodrato and Vione, 2014), as shown in Equation (5) .

$$k_{Phot} = \frac{1}{0.1z}\int \Phi(\lambda)\varepsilon(\lambda)p^0(\lambda)\cdot\frac{1-10^{-100\alpha(\lambda)z}}{\alpha(\lambda)}d\lambda \quad (5)$$

Noted that k_{Phot} determined by Equation (5) is not the rate constant at depth z but the average rate constant of a water column of depth z, taking into account the attenuation of sunlight through the optical path based on Beer-Lambert's Law. Complete vertical mixing is assumed, i.e., the water chemistry along the optical path is uniform. This assumption is valid for maturation pond, as it usually shows less vertical biological and physicochemical stratification (Kayombo et al., 2005). $p^0(\lambda)$ is the photon flux density of the sunlight incident on water surface, in $Einstein\cdot cm^{-2}\cdot s^{-1}\cdot nm^{-1}$. APEX model can estimate $\alpha(\lambda)$ as an exponential function of wavelength with a scale factor of DOC concentration in water. Ranges of other parameters for the estimation of $\alpha(\lambda)$ of typical natural surface water and WSP water were provided in the program (Bodrato and Vione, 2014). $\varepsilon(\lambda)$ indicates the relative probability of absorption of photons at different wavelengths by viral components, while $\Phi(\lambda)$ represents the likelihood of the absorbed photons causing inactivation. Mattle et al. (2015) estimated and reported values of $\varepsilon(\lambda)$ and Φ for MS2 bacteriophage, adenovirus and phiX174. Kohn et al. (2016) compared the k_{endo} estimated based on wavelength-dependent quantum yield $\Phi(\lambda)$ verses constant quantum yield Φ, and concluded that quantum yields of viruses are independent of wavelengths. Prediction of this model generally showed good agreements with observed apparent inactivation

rate constants of MS2 and phiX174, yet it tended to underestimate the total inactivation rate constant of adenovirus. However, a comparative analysis by Silverman et al. (2019) find that the proposed quantum yield leads to an overestimation of k_{endo} of MS2, and the authors provided suggestions for parameter calibration to better fit the measured data.

2.2.2 Indirect exogenous inactivation

MS2, PRD1, rotavirus, adenovirus and PV3 were shown to be susceptible to indirect exogenous inactivation (Kohn and Nelson, 2007; Love et al., 2010; Romero-Maraccini et al., 2013; Romero et al., 2011; Silverman et al., 2015; Sinton et al., 2002). Nelson et al. (2018) reviewed and summarized the relevant photochemical reactions in solar inactivation. CDOM, absorbing sunlight over the UVB, UVA and visible light range, is the most important exogenous photosensitizer in the environment. Upon absorption of sunlight photon, CDOM is promoted to an excited singlet state ^{1}CDOM*, most of which shortly emits heart or light and returns to the ground state. Some ^{1}CDOM* could reach a long-lived excited triplet state (^{3}CDOM*) through intersystem crossing. In addition to directly oxidizing some viral component as a PPRI to cause inactivation, ^{3}CDOM* can sensitize other water constituents (e.g. DO) and facilitate the production of other PPRIs. ROS is the most important group of PPRIs, including singlet oxygen ($^1O_2$), superoxide ($O_2^{\bullet-}$), hydrogen peroxide (H_2O_2) and hydroxyl radical ($^{\bullet}OH$). The formation of ROS often involves transferring energy from photon or other energized species (e.g. ^{3}CDOM*) to DO. Particularly, $^{\bullet}OH$ can also form through photolysis of nitrate or nitrite and photo-Fenton reaction involving Fe (III) and H_2O_2. Several studies found that the inactivation of MS2 was dominated by $^1O_2$ (Kohn et al., 2007; Kohn and Nelson, 2007) and a linear correlation was observed between the observed MS2 inactivation rate constant and the concentration of ROS (Rosado-Lausell et al., 2013). Carbonate radical ($CO_3^{\bullet-}$) and reactive halogen species are also potential to cause exogenous inactivation as PPRIs.

The susceptibility of virus to each PPRI depends on the abundance, accessibility and higher structure of viral components containing reactive sites. Complex mechanisms of biological repair and the redundancy of non-vital reactive sites also influence the apparent susceptibility of a virus species to a certain PPRI. Existing studies suggest that the exogenous inactivation process can be modeled as a series of parallel second-order reaction between virus and PPRIs (Equation (6)).

$$k_{exo} = \sum_{\text{PPRI}} k_{\text{virus,PPRI}} \cdot [\text{PPRI}]_{\text{ss}} \quad (6)$$

where the $k_{\text{virus,PPRI}}$ indicates the susceptibility of a virus to a certain PPRI. $[\text{PPRI}]_{\text{ss}}$ is the steady-state concentration of the PPRI, which depends on the photochemical reactions and the physicochemical conditions in the water. This form was also adopted by Bodrato and Vione (2014) primarily for the modeling of photochemical transformation kinetics of xenobiotics in surface waters. Same was used in Silverman et al.'s (2019a) model of sunlight-mediated removal of trace organic and microbial contaminants in treatment wetlands. Different between the two studies is the prediction of $[\text{PPRI}]_{\text{ss}}$.

In APEX model (Bodrato and Vione, 2014), four PPRIs are considered: ^{3}CDOM*, $^1O_2$, $^{\bullet}$OH and $CO_3^{\bullet-}$. The steady-state concentration of each PPRI is determined by the equilibrium between the formation and scavenging process of the species, which depends on the water chemistry (concentrations of CDOM, DOC, CO_3^{2-}, HCO_3^-, NO_3^-, NO_2^-, and Br^-), water depth, and the angle and spectrum of incident sunlight (Figure 1). Although the model does not explicitly include pH as a parameter, the influence of pH on the photochemistry can be partially examined through the pH-dependent speciation of carbonates. As the model adopted a fixed value of the pseudo first-order $^1O_2$ formation rate constant, it excluded the impact of DO from the prediction of exogenous inactivation rate constant by assuming there is constant amount of DO available for the formation of $^1O_2$. Both Kohn et al. (2016) and Mattle et al. (2015) adopted this model in investigating the inactivation of MS2, adenovirus and phiX174, whose second-order inactivation rate constants with PPRIs were estimated with experimental data.

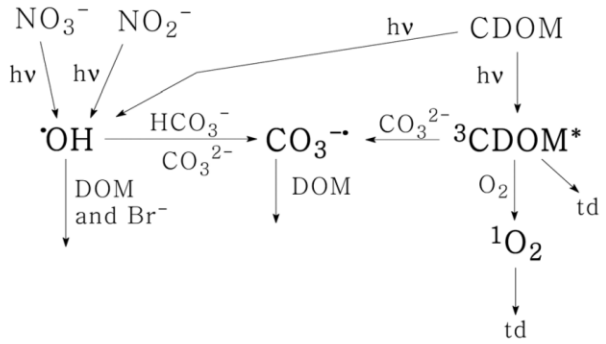

Figure 1. An overall scheme of main photochemical reactions in APEX model (Bodrato and Vione, 2014)

Because $^1O_2$ was found to be the most important PPRI for the inactivation of MS2 in multiple experimental settings and the measured k_{exo} was observed to scale with $[^1O_2]_{ss}$ (Kohn and Nelson, 2007; Rosado-Lausell et al., 2013; Silverman et al., 2013), Silverman et al. (2019a) used $[^1O_2]_{ss}$ as the single indicator for overall exogenous inactivation, suggesting the second-order inactivation rate constant between virus and $^1O_2$ varies across different waters. And $[^1O_2]_{ss}$ was determined as proportional to the concentration of DOC (Equation (7)) based on previous observations of $[^1O_2]_{ss}$ and [DOC] in near-surface effluent dominated water at noon in summer. This model provides a simple tool for the prediction of MS2 inactivation rate constant from a statistical modeling prospective, but it may not be general for different virus species, water chemistry or sunlight irradiance spectra.

$$[^1O_2]_{ss} = \frac{1\times10^{-14}\,\mathrm{M\cdot L-C}}{\mathrm{mg}} \cdot [\mathrm{DOC}] \cdot \frac{E_{24\mathrm{h\ avg}}(\lambda=410\ \mathrm{nm})\cdot S(\lambda=410\ \mathrm{nm},z)}{1.22\ \mathrm{W/m^2}} \quad (7)$$

So far, temperature has yet been incorporated into existing mechanistic solar virus inactivation models. Although neither of the two models capture every aspect of solar virus inactivation, they provide practical tools for the estimation of $[\mathrm{PPRI}]_{ss}$ based on the physicochemical conditions that are easy to measure.

2.3 Need for prioritizing influential factors

2.3.1 Uncertainties in solar virus inactivation

In the past decades, studies investigating the wastewater treatment systems utilizing sunlight-mediated inactivation have reported highly variable virus removal efficiencies. Victor et al. (2006) reviewed relevant studies from 1983 to 2005 and found that achieved removal of viruses varies from 1-log to 4-log for WSPs and treatment reservoirs and up to 2-log for constructed wetlands. Verbyla et al. (2017) found the highest virus removal (0.9-log on average) can be achieved in maturation ponds, which still ranged from negligible level to 1.8-log at maximum. The uncertainty of the pathogen removal performance of a system is caused by a wide range of factors simultaneously. It is impossible to identify a single determinant factor (Oliveira and von Sperling, 2011).

Great efforts have been made to investigate some factors impacting the pathogen removal efficiency of these systems (Badrot-Nico et al., 2009; Dahl et al., 2017; Dias et al., 2017; Li et

al., 2018; Liu et al., 2016; Ouali et al., 2015; Verbyla et al., 2017). A lot of them focused on the design factors influential on the hydraulic efficiency or simply the hydraulic retention time of the system, yet they failed to investigate the interaction effect between the design factors and the sunlight exposure. So, the conclusions regarding these design factors are not specific to pathogen removal through solar inactivation and could be biased. With the progress made in mechanistic understanding of solar virus inactivation, some studies examined the impacts of several factors on solar inactivation rate constants through modeling and experiments (Kohn et al., 2016; Mattle et al., 2015). Due to the physical limitations of experiments, the uncertainty space of the factors involved in solar virus inactivation is hardly ever fully examined. Interactions among multiple factors are seldom revealed by limited number of different experimental settings.

To provide accurate information to effectively improve the pathogen removal efficiency of the systems, it is essential to identify the factors (as well as their correlations) involved in the determination of solar virus inactivation rate and elucidate the relative importance of these factors. Given the complexity of the processes and the large number of factors involved, such objectives can only be achieved through computational experiments on the mechanistic model (i.e., uncertainty analysis and sensitivity analysis).

2.3.2 Global sensitivity analysis for factor prioritization

Sensitivity analysis is commonly used to determine which inputs have important effects on the output of a complicated deterministic model (Morris, 1991). The sensitivity to a certain input factor is determined by the model structure as well as the multivariate distribution of the input factors. Potential questions that can be answered by sensitivity analysis include: 1) Which input factors should one prioritize to reduce the uncertainty of the output by fixing the fewest factors at their true values? 2) Which input factors are not influential to the output so that one can fix them without worrying about the prediction accuracy of the model? 3) How do one reduce the output variance to a certain level by eliminating the uncertainties of some input factors? 4) Which factor is most responsible for producing realization of output in the region of interest? These questions respectively correspond to four different settings of sensitivity analysis: factors prioritization (FP), factors fixing (FF), variance cutting (VC) and factors mapping (FM). They represent different goals and applications of sensitivity analysis (Saltelli, 2002).

Global sensitivity analysis (GSA), compared to local sensitivity analysis, is capable of capturing the overall influence of individual input factors as well as the influence of interactions between them by exploring their whole variation space (Iooss and Lemaitre, 2015). It has become more and more popular as a computational method for the measurement of importance. Diversities of GSA methods have been developed since 1990s, several of which have been widely recognized and applied. In the context of identifying factors that most need better determination, GSA is often performed using techniques based on linear regression or correlation, such as Pearson correlation coefficient, standard regression coefficient and partial correlation coefficient. If the model is non-linear, Spearman correlation coefficient, standardized rank regression coefficient and partial rank correlation coefficient can serve as substitute indices by replacing sample data with their ranks in calculation. However, regression-based methods can give totally misleading results if the requirement of monotonic model is not met. Screening technique, variance-based methods and Monte Carlo filtering (MCF) stand out as GSAs independent from assumptions about the model. MCF identify the parameters that are most responsible for producing acceptable outputs by performing two-sided Smirnov tests for each factor, whose two samples are classified according to whether it is associated with an acceptable output. It is tailored for the factors mapping setting and convenient for model calibration.

Morris (1991) firstly proposed using the mean and standard deviation of elementary effects as indicators to classify input factors into three groups (Morris OAT method): inputs having negligible effects on the output, inputs having large linear effects without interactions, and inputs having large non-linear and/or interaction effects. Elementary effects of input factors are calculated by varying one factor at a time in random order in the input space. Morris method is the most widely used screening technique. Campolongo et al. (2007) refined Morris method by introducing another sensitivity index μ^* (i.e., mean of the absolute values of elementary effects) and improving the sampling strategy to ensure better scanning of the input space without increasing the number of model executions needed. Morris method is among the most efficient model-free GSA methods. It can provide qualitative information for factors fixing setting at a relatively low computational cost, but it tends to be less robust compared to variance-based methods since the relative importance of different inputs is not quantified (Gan et al., 2014).

Inspired by classical ANOVA, variance-based sensitivity indices were proposed as nonparametric measures of importance, which apportion the output variance to different effects of input uncertainties (McKay et al., 1999). First-order effect of input j (i.e., main effect, S_j) measures the share of output variance caused by the uncertainty of input j alone. It is convenient in factors prioritization setting. Total effect S_{Tj} indicates the share of output caused by the uncertainty of j and all the interactions between j and other inputs in the model. It is mostly used in variance cutting setting and factor fixing setting. Sobol' method (1993) defines a procedure for economical sampling and estimation of the variance-based sensitivity indices based on ANOVA. A robust estimation of Sobol' indices requires a much larger sample than screening techniques. Fourier amplitude sensitivity test (FAST) is able to estimate S_j at a lower computational cost than Sobol' method, i.e., FAST is more robust at low sample size. Saltelli et al. (1999) introduced a new GSA method based on FAST that allows estimation of total effects with same computational efficiency. But Sobol' method is superior to FAST in that it allows the computation of higher-order interaction effects, e.g. it can estimate main effects, second-order interaction effects and total effects of k inputs at a total cost of $N(2k + 2)$ samples, where $N = 10^4$ is required in common practice (Iooss and Lemaitre, 2015).

Selection of GSA methods depends on the properties of the model, the computational capacity as well as the purpose of sensitivity analysis. Cariboni et al. (2007) and Gan et al. (2014) both provided a decision diagram for the choice of an SA method based on these considerations. Morris Method and Sobol' indices are suitable for non-linear models and most settings (FF, FP, and VC).

CHAPTER 3: METHODS, RESULTS AND DISCUSSION

3.1 Methodology

3.1.1 Global sensitivity analyses – Morris OAT screening and Sobol' variance-based indices

To elucidate the relative importance of various input parameters on solar virus inactivation, global sensitivity analysis based on two different methods were performed: Morris one-at-a-time (OAT) screening technique was firstly used to rank the parameters according to their relative influences and to identify the unimportant parameters; Sobol' method was then chosen to quantify the relative importance of these parameters. Both methods are global, model-independent and robust given an adequate sample size.

Morris OAT method estimates two sensitivity indices μ_i^* and σ_i using model input and output data. Index μ_i^* indicates the overall influence of x_i on y (Campolongo et al., 2007). σ_i detects whether x_i is involved in interaction with other input variables. A larger σ_i implies stronger interactions between x_i and other input variables, and thus, a higher non-linearity of the model. To derive the two sensitivity indices, independent input parameters x_i (i = 1, 2, ..., k) of the model are varied one at a time within their value ranges in a random order to obtain a number of sampling points $\boldsymbol{X}^j$ (j = 1, 2, …, r) in the input space, which are used to compute the elementary effect $d_i(\boldsymbol{X}^j)$ of each parameter x_i.

$$d_i(\boldsymbol{X}^j) = \frac{y(x_1^j, \dots, x_i^j + \Delta, \dots, x_k^j) - y(x_1^j, \dots, x_i^j, \dots, x_k^j)}{\Delta} \tag{8}$$

$$\mu_i^* = \frac{1}{r}\sum_{j=1}^{r} |d_i(\boldsymbol{X}^j)| \tag{9}$$

$$\mu_i = \frac{1}{r}\sum_{j=1}^{r} d_i(\boldsymbol{X}^j) \tag{10}$$

$$\sigma_i = \sqrt{\frac{1}{r}\sum_{j=1}^{r}(d_i(\boldsymbol{X}^j) - \mu_i)^2} \tag{11}$$

The most efficient sampling design suggested by Morris (1991) for this method is to randomly construct *r* walking trajectories in the input space, each one of which includes *k* steps and produces one elementary effect for each of the *k* input variables. The construction of trajectories was implemented through random sampling of *r* orientation matrices $\boldsymbol{B}^*$, the technique of which was introduced in detail by Saltelli et al. (2004). Before sampling and calculation of indices, all input parameters of the model were scaled to the interval [0, 1] for the simplicity of matrix construction. 18,000 simulations based on 1,000 random trajectories were performed to calculate Morris sensitivity indices for each combination of virus species and water type.

After Morris screening, Sobol' variance-based sensitivity indices were estimated to quantitatively attribute the uncertainty of the pseudo 1st-order solar virus inactivation rate constant (k_{total}) to the uncertainties of different input parameters (Table 1). Sobol' method can capture the influence of the shape and range of the probability distributions of inputs and appreciate the interaction effect of inputs. For models with orthogonal inputs, the uncertainty of output y can be decomposed as follows:

$$V(y) = \sum_i V_i + \sum_i \sum_{m>i} V_{im} + \cdots + V_{12\ldots k} \tag{12}$$

where $V_i = Var\big(E(y|x_i)\big)$, $V_{im} = Var\big(E(y|x_i, x_m)\big) - V_i - V_m$. Total effect of x_i on y can also be decomposed as:

$$V(y) - Var\big(E(y|X_{-i})\big) = V_i + \sum_{m\neq i} V_{im} + \sum_{p\neq m\neq i} V_{imp} + \cdots + V_{12\ldots k} \tag{13}$$

where X_{-i} means fixing all input parameters but x_i. Normalization of Equation (13) with $V(y)$ yields:

$$S_{Ti} = S_i + \sum_{m\neq i} S_{im} + \cdots + S_{12\ldots k} \tag{14}$$

where S_i, main effect, indicates the uncertainty of y that is removed by fixing x_i at its true value, and S_{im}, second-order interaction effect, implies the influence of interaction between x_i and x_m on y, and so forth. Regardless of interaction and non-orthogonality, S_i serves as a proper measure of the importance of an input parameter (Saltelli et al., 2004). In this study, S_i, S_{Ti} and S_{im} were estimated to characterize the relative importance of 15 orthogonal parameters.

To minimize computation cost, an empirical sampling procedure specific for orthogonal input variables was adopted (Saltelli et al., 2004; Sobol', 1993). Two $N \times k$ matrices $\mathbf{M}_0$ (sample matrix) and $\mathbf{M}_0'$ (resample matrix) were independently constructed through Monte Carlo sampling in the input space, and their output vectors were denoted as $\mathbf{Y}_0$ and $\mathbf{Y}_0'$ respectively:

$$\mathbf{M}_0 = \begin{pmatrix} x_1^{(1)} & x_2^{(1)} & \cdots & x_k^{(1)} \\ x_1^{(2)} & x_2^{(2)} & \cdots & x_k^{(2)} \\ \vdots & \vdots & \cdots & \vdots \\ x_1^{(N)} & x_2^{(N)} & \cdots & x_k^{(N)} \end{pmatrix} \tag{15}$$

$$\mathbf{Y}_0 = \left(y_0^{(1)}, y_0^{(2)}, \ldots, y_0^{(N)}\right)^{\mathbf{T}} \tag{16}$$

$$\mathbf{M}_0' = \begin{pmatrix} x_1^{(1')} & x_2^{(1')} & \cdots & x_k^{(1')} \\ x_1^{(2')} & x_2^{(2')} & \cdots & x_k^{(2')} \\ \vdots & \vdots & \cdots & \vdots \\ x_1^{(N')} & x_2^{(N')} & \cdots & x_k^{(N')} \end{pmatrix} \tag{17}$$

$$\mathbf{Y}_0' = \left(y_0^{(1')}, y_0^{(2')}, \ldots, y_0^{(N')}\right)^{\mathbf{T}} \tag{18}$$

By switching the i-th columns in $\mathbf{M}_0$ and $\mathbf{M}_0'$, new input matrices $\mathbf{N}_i$, $\mathbf{N}_{-i}$ (i = 1, 2, …, k) were constructed, whose corresponding outputs were $\mathbf{Y}_i$ and $\mathbf{Y}_{-i}$:

$$\mathbf{N}_i = \begin{pmatrix} x_1^{(1')} & \cdots & x_i^{(1)} & \cdots & x_k^{(1')} \\ \vdots & & \vdots & & \vdots \\ x_1^{(N')} & \cdots & x_i^{(N)} & \cdots & x_k^{(N')} \end{pmatrix} \tag{19}$$

$$\mathbf{Y}_i = \left(y_i^{(1)}, y_i^{(2)}, \ldots, y_i^{(N)}\right)^{\mathbf{T}} \tag{20}$$

$$\mathbf{N}_{-i} = \begin{pmatrix} x_1^{(1)} & \cdots & x_i^{(1')} & \cdots & x_k^{(1)} \\ \vdots & & \vdots & & \vdots \\ x_1^{(N)} & \cdots & x_i^{(N')} & \cdots & x_k^{(N)} \end{pmatrix} \tag{21}$$

$$\mathbf{Y}_{-i} = \left(y_{-i}^{(1)}, y_{-i}^{(2)}, \ldots, y_{-i}^{(N)}\right)^{\mathbf{T}} \tag{22}$$

$\mathbf{M}_0$, $\mathbf{M}_0'$, $\mathbf{N}_i$, and $\mathbf{N}_{-i}$ (i = 1, 2, …, k) together yields N·(2k+2) output values in total, with which Sobol' indices were computed as follows:

$$S_i = \frac{Var\left(E(y|x_i)\right)}{V(y)} = \frac{u_i - \mu^2}{\sigma^2} \tag{23}$$

$$S_{Ti} = 1 - \frac{Var\left(E(y|X_{-i})\right)}{V(y)} = 1 - \frac{u_{-i} - \mu^2}{\sigma^2} \tag{24}$$

where

$$\hat{\mu} = \frac{1}{N(2k+2)} \sum_{r=1}^{N(2k+2)} y^{(r)} \tag{25}$$

$$\widehat{\sigma^2} = \frac{1}{N(2k+2)-1} \sum_{r=1}^{N(2k+2)} \left[\left(y^{(r)}\right)^2 - \hat{\mu}^2\right] \tag{26}$$

$$\widehat{u_\iota} = \frac{1}{N-1} \sum_{r=1}^{N} y_0^{(r)} \cdot y_i^{(r)} \tag{27}$$

$$\widehat{u_{-\iota}} = \frac{1}{N-1} \sum_{r=1}^{N} y_0^{(r)} \cdot y_{-i}^{(r)} \tag{28}$$

To learn the effect of interactions between any two input variables, the second-order interaction effect indices S_{im} were estimated as follows. For any $i \neq m$,

$$S_{im} = \frac{Var\left(E(y|x_i, x_m)\right)}{V(y)} - S_i - S_m = \frac{u_{im} - \mu^2}{\sigma^2} - S_i - S_m \tag{29}$$

where

$$\widehat{u_{im}} = \frac{1}{N-1}\sum_{r=1}^{N} y_{-i}^{(r)} \cdot y_{m}^{(r)} \quad (30)$$

This study set $N = 10^4$ and performed 320,000 simulations for each combination of virus and water type to estimate the Sobol' indices of the 15 parameters with acceptable uncertainty (Iooss and Lemaitre, 2015; Saltelli et al., 2004). Python module SALib was used for the execution of sampling and analyses for Morris and Sobol' methods (Herman and Usher, 2017).

3.1.2 Integrated modeling of solar virus inactivation

Incorporating sunlight irradiance model into the prediction of solar virus inactivation allows us to investigate the influence of independent environmental parameters. The modelling of sunlight irradiance incident on water surface was conducted leveraging the SMARTS program (Gueymard, 1995). SMARTS was shown to be able to model sunlight irradiances in good agreement with various measured datasets, but it tended to overestimate UVB region irradiance without considering cloud cover (Apell and McNeill, 2019). To model the empirical sunlight radiation but reduce the complexity of subsequent global sensitivity analysis, the input values of geographical parameters (latitude, longitude and altitude), temporal parameters (date and hour) and some atmospheric condition parameters (e.g. turbidity, CO_2 concentration) were customized, while default values provided in the program were adopted for atmospheres, extraterrestrial spectrum and aerosol models (Appendix A). Local sunlight photon flux density profile $p^0(\lambda)$ [$cm^{-2}{\cdot}s^{-1}{\cdot}nm^{-1}$] as well as zenith angle [°] were the outputs of interest and were input to the photochemical reaction model after unit conversion (Figure 2).

APEX (Bodrato and Vione, 2014) was adapted to model the solar virus inactivation because it is currently the most comprehensive photochemistry model for natural water, and it has been verified by a few studies regarding solar virus inactivation and chemical degradation (De Laurentiis et al., 2013; Mattle et al., 2015). Quantum yields Φ_{virus} [unitless] and molar absorption coefficients $\varepsilon_{virus}(\lambda)$ [$M^{-1}{\cdot}cm^{-1}$] were adjusted according to virus species in the prediction of direct photolysis rate constant k_{endo}. Second-order reaction rate constants $k_{virus,PPRI}$ [$M^{-1}{\cdot}s^{-1}$] between viruses and PPRIs ($^1O_2$, $^{\bullet}OH$, $CO_3^{\bullet-}$, $^3CDOM^*$) were used in the prediction of k_{exo}. Water quality parameters varied based on water types and affected the

prediction of steady-state concentrations of PPRIs (i.e.,$[PPRI]_{ss}$). Sunlight attenuation through water body was taken into consideration by averaging values over the depth of a well-mixed water column. Major equations for the prediction of total inactivation rate constant are:

$$k_{total} = k_{endo} + k_{exo} \tag{31}$$

$$k_{endo} = \int_{\lambda} \Phi_{virus}\varepsilon_{virus}(\lambda) \cdot p^0(\lambda) \cdot \frac{1 - 10^{-100A_1(\lambda)l}}{A_1(\lambda)l} d\lambda \tag{32}$$

$$k_{exo} = \sum_{PPRI} k_{virus,PPRI}[PPRI]_{ss} \tag{33}$$

Differing from z in Equation (5), l in Equation (32) represents optical path length of the water column, derived as a function of incident zenith angle and water depth. With incident sunlight spectrum and solar position data from SMARTS program, optical path length correction is automated by modifying the program codes regarding water depth. $A_1(\lambda)$ [cm^{-1}], the specific water absorbance over a 1 cm optical path, was predicted as an exponential function of NPOC (non-purgeable organic carbon, same as dissolved organic carbon, DOC) concentration and wavelength:

$$A_1(\lambda) = \alpha \cdot [NPOC] \cdot e^{-\beta\lambda} \tag{34}$$

Standard time unit of model outputs is hour, converted from summer sunny day (SSD) in APEX, which corresponds to fair-weather July 15th at 45 °N latitude. Because the integrated model has incorporated temporal variables in sunlight irradiance prediction, seasonal variation correction in the APEX program was omitted.

In this study, pH, water temperature, and DO are not included as variables in GSA of the integrated solar virus inactivation model, because previous studies have shown that the inactivation by pH or temperature alone is usually insignificant in natural water and WSPs (Davies-Colley, 2005; Dias et al., 2017; Maiga et al., 2009). Neither the relation between pH, DO and the formation of PPRIs or the effect of temperature on solar virus inactivation rate constants has been quantified. This study also assumed sunlight absorbance by algae and cyanobacteria is minimal compared to CDOM in both water types.

3.1.3 Uncertainties of input parameters

In this study, the relative importance of 15 parameters characterizing the environmental factors, water quality, virus susceptibility and engineering design of the reaction systems in the integrated solar virus inactivation model were compared. Geographical location, elevation, seasonal and diurnal motion affect the solar virus inactivation by determining the solar position and accordingly the sunlight irradiance incident on water surface. While latitude, longitude and altitude were treated as independent variables in simulations for Morris method, empirical elevation data was randomly sampled from the land area between 60° S and 60° N using the SRTM dataset (1 km resolution) in simulations for Sobol' method (Jarvis et al., 2008). Simulations were run on the 22nd across 12 months between the sunrise and sunset time specific to the location and the season. Concentrations of NPOC, nitrate and nitrite as well as the absorbance spectrum of water were varied in simulation as they are major photosensitizers to the production of several PPRIs. NPOC is also the main sunlight absorber in WSP (Kohn et al., 2016). Molar absorption coefficient and quantum yield of viruses indicates the virus susceptibility to endogenous inactivation and 2nd-order reaction rate constants indicates the resistance of viruses to different reactive species. Water depth was chosen as a key engineering design parameter in sensitivity analysis, as it determines the optical path length and sunlight attenuation. Other design parameters do not directly affect solar virus inactivation. Uncertainties of the parameters were determined based on existing studies and expert opinions. Distributions of independent parameters for Monte Carlo sampling are summarized in Table 1.

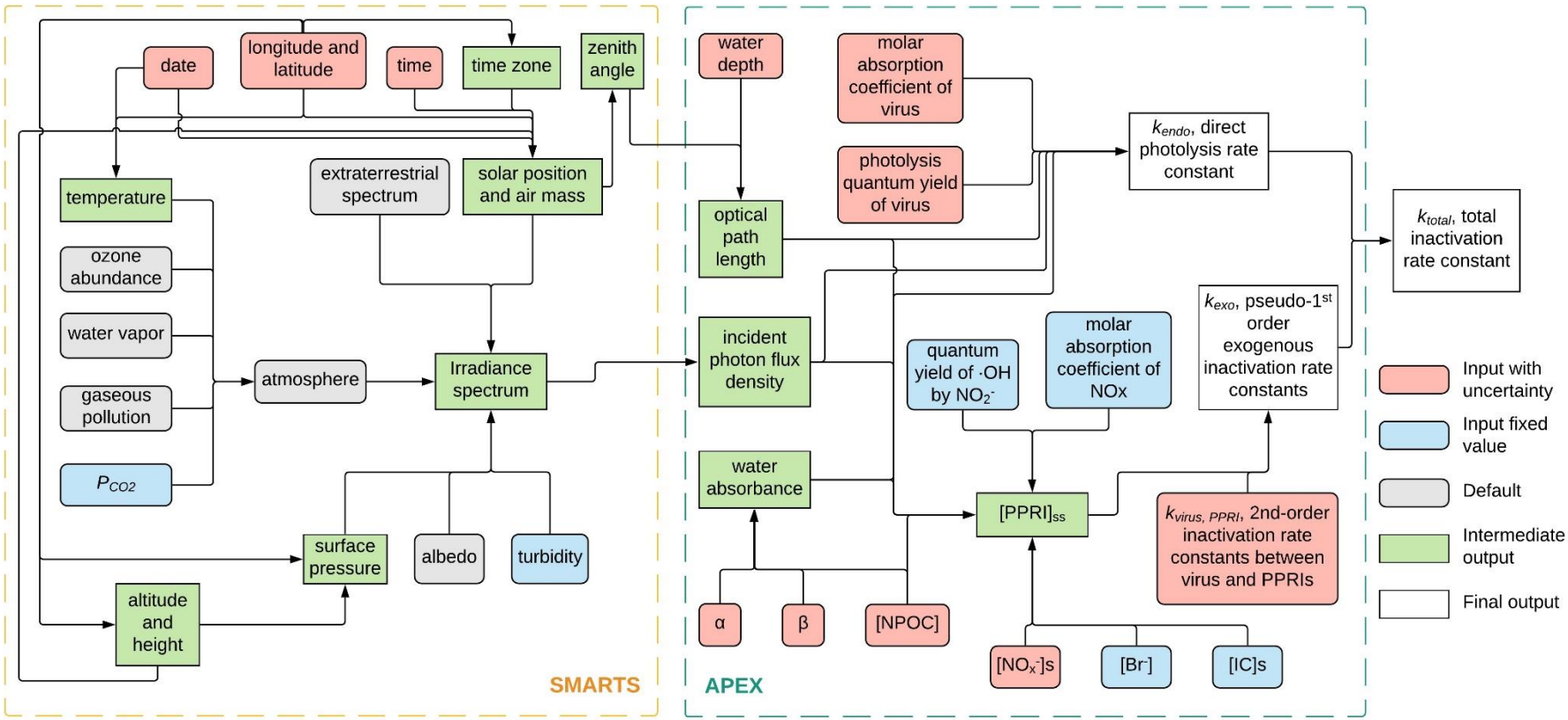

Figure 2. Schematic flow chart of the integrated solar virus inactivation model

Table 1. Distributions of input parameters in sensitivity analyses

Category	Parameter	Unit	Distribution	Values	Citation[d]
Environmental	Month	unitless	discrete uniform	{1, 2, 3, 4, 5, 6, 7, 8, 9, 10, 11, 12}	-
	Hour[a]	unitless	uniform	between sunrise and sunset	-
	Latitude[b]	°	uniform or empirical	-60, 60	
	Longitude[b]	°	uniform or empirical	-180, 180	1
	Altitude[c]	km	uniform or empirical	0, 3.5	
Water quality	α	unitless	uniform	0.41, 0.49 (natural water); 0.14, 0.22 (WSP water)	2
	β	unitless	uniform	0.013, 0.017 (natural water); 0.011, 0.015 (WSP water)	2
	[NPOC]	mg-C·L^{-1}	uniform	1, 40	3 - 14
	[NO_3^-]	M	uniform	1.13E-5, 9.84E-4	4, 5, 8, 9, 11, 15
	[NO_2^-]	M	uniform	1.20E-5, 7.20E-4	5, 9, 11, 13
Photo-reactivity	$k_{virus,\cdot OH}$	10^9 M^{-1}·s^{-1}	uniform	2.8, 5.6 (Adenovirus)	5, 9
				5.5, 9.3 (MS2)	5, 9
				1.0, 2.4 (ΦX174)	5, 9
	$k_{virus,CO_3^{\cdot-}}$	10^8 M^{-1}·s^{-1}	uniform	0.5, 1.1 (Adenovirus)	5, 9
				1.0, 1.6 (MS2)	5, 9
				0.3, 0.9 (ΦX174)	5, 9
	$k_{virus,^1O_2}$	10^8 M^{-1}·s^{-1}	uniform	1.8, 2.6 (Adenovirus)	5, 9
				1.2, 19.7 (MS2)	5, 6, 9, 13, 16, 17
				0.47, 0.69 (ΦX174)	5, 9
	$k_{virus,^3CDOM^*}$	10^8 M^{-1}·s^{-1}	uniform	0.4, 1.0 (Adenovirus)	5, 9
				4.7, 31.7 (MS2)	5, 9, 13, 14
				0.12, 0.22 (ΦX174)	5, 9
	ε_{virus}	M^{-1}·cm^{-1}	uniform	±50%	5, 9
	Φ_{virus}	unitless	uniform	2.0e-4, 3.0e-4 (Adenovirus)	5, 9
				1.28E-4, 3.84E-4 (MS2)	18
				1.3E-2, 1.5E-2 (ΦX174)	5, 9
Engineering design	Water depth	m	uniform	0.01, 3	5

a. Hour was sampled randomly between the sunrise time and the sunset time, which was predicted based on location, elevation and date.

b. Latitude and longitude were jointly sampled from the land area in the SRTM dataset in simulations for Sobol' method.

c. Altitude was determined by latitude and longitude in simulations for Sobol' method, using empirical data from the SRTM dataset. Latitude, longitude and altitude were grouped and analyzed as one parameter, location, in Sobol' method.

d. Citation: 1- Jarvis et al., 2008; 2 - Bodrato and Vione, 2014; 3 - Boehm et al., 2009; 4 - Carratalà et al., 2016; 5 - Kohn et al., 2016; 6 - Kohn et al., 2007; 8 - Mamane et al., 2007; 9 - Mattle et al., 2015; 10 - Nguyen et al., 2014; 11 - Romero-Maraccini et al., 2013; 12 - Romero et al., 2011; 13 - Rosado-Lausell et al., 2013; 14 - Silverman et al., 2015; 15 - Mian et al., 2010; 16 - Kohn and Nelson, 2007; 17 - Silverman et al., 2013; 18 - Silverman et al., 2019.

3.1.4 Modeling of MS2 log removal of a maturation pond system

A 3-D CSTR model was used to simulate the sunlight-mediated virus inactivation in a maturation pond with dimensions shown in Figure 3. The four walls of the maturation pond were assumed to be vertical and of equal height for a conservative prediction of virus removal performance. Equation (35) defines the volume of the maturation pond.

$$V = L \cdot W \cdot D \tag{35}$$

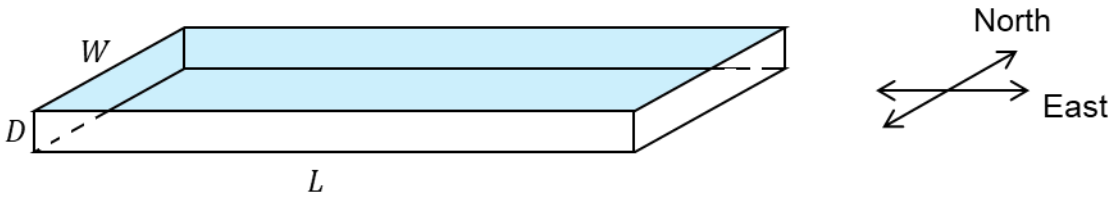

Figure 3. Dimensions of the maturation pond. L was assumed to always be aligned with the line of latitude in simulations, and W was always aligned with the line of longitude. The relative lengths of the walls are determined by the $L/$W ratio. The pond depth is denoted as D.

Sunlight spectra were predicted every hour between sunrise and sunset using SMARTS. It was assumed that within each hour, the sunlight spectrum, and thus, the inactivation rate constant remains constant. Because inactivation usually takes more than one hour to reach steady state, the reactor kinetics within each hour of constant sunlight irradiation is described by Equation (36)-(38) as a function of reaction time t. In the simulations, when the difference of effluent concentrations at the same time on two consecutive days dropped below 0.1%, the inactivation of the maturation pond was considered at equilibrium (see Figure 4 for example). The effluent concentrations of last 24 hours were used to calculate the log removal of the maturation pond.

$$\frac{N_t}{N_{in}} = \frac{N_0}{N_{in}} \cdot e^{-at} + \frac{b}{a}(1 - e^{-at}) \tag{36}$$

$$a = \frac{1}{t_R} + \hat{k} \tag{37}$$

$$b = \frac{1}{t_R} \tag{38}$$

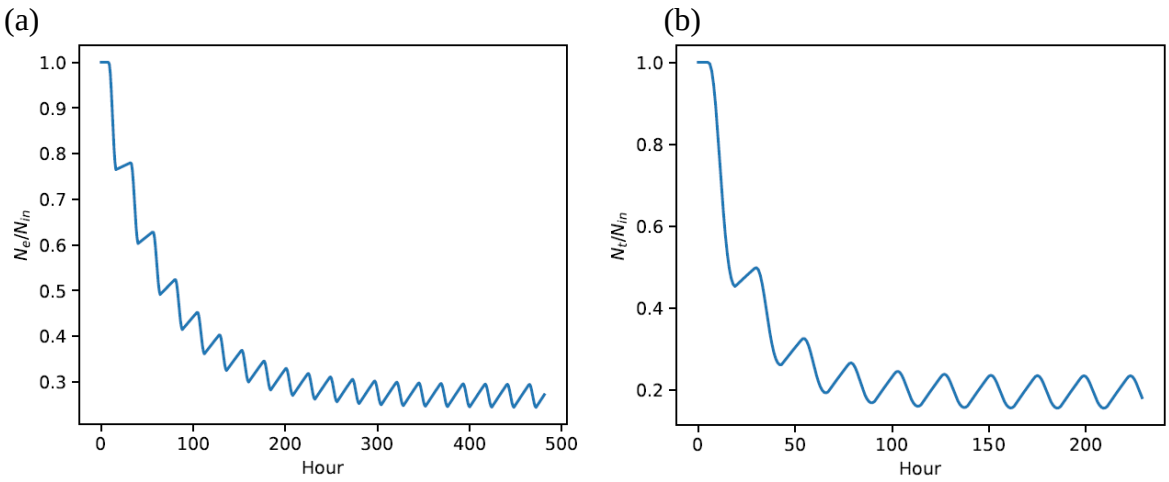

Figure 4. Examples of simulated effluent MS2 concentration profile. (a) HRT = 10 days, d = 1.5 m, December 22nd; (b) HRT =5 days, d = 1.5 m, June 22nd

N_t [m^{-3}] is the effluent virus concentration after t hour of inactivation by the constant sunlight irradiation. N_{in} [m^{-3}] is the influent virus concentration, which was assumed to be constant in simulation. N_0 [m^{-3}] is the initial effluent virus concentration at the beginning of the hour. t_R [h] is the theoretical hydraulic retention time of the maturation pond. $\hat{k}$ is the apparent solar inactivation rate constant, which was affected by the geometric relations between the incident sunlight and the pond design. Estimations of $\hat{k}$ are summarized as follows. Direction of the incident sunlight was described simultaneously by z, zenith angle and φ, azimuth angle, as shown in Figure 5(a). Due to refraction by the water body, a relation between the zenith angle and the angle of the optical path in water can be described by Equation (39), where n is approximately 1.34 for water.

$$\sin\eta = \frac{\sin z}{n} \tag{39}$$

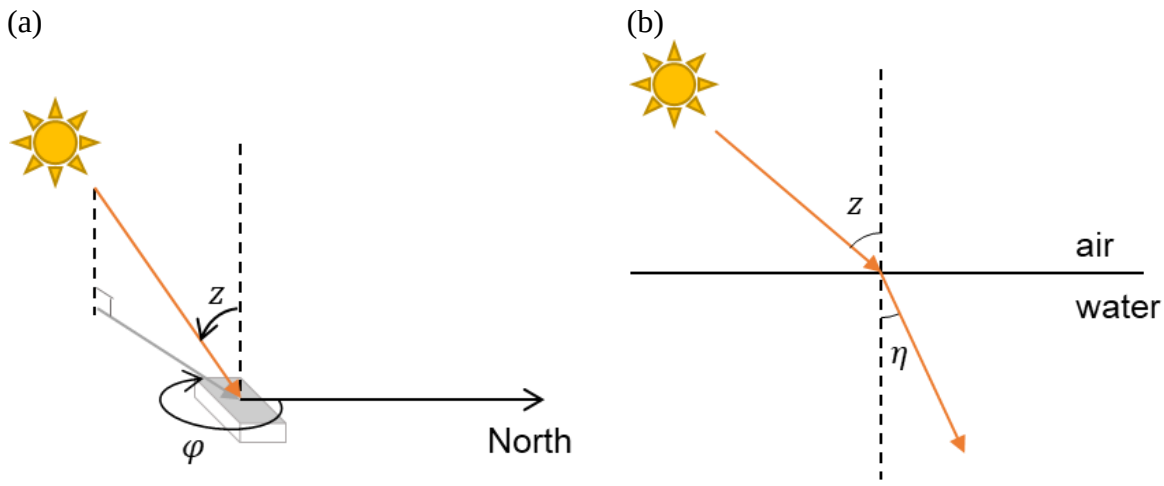

Figure 5. (a) Sunlight irradiation on pond surface and (b) sunlight refraction through water body. z is the zenith angle and φ is the azimuth angle of the incident sunlight.

As shown in Figure 6, when $L < W|\tan\varphi|$, $\hat{k}$ was estimated using Equations (40)-(42), before which φ, if falls in (180°, 360], was converted to (0°, 180°] by subtracting 180°. $k(h,\eta)$ represents the total inactivation rate constant predicted by the integrated solar virus inactivation model when water depth is h and angle of the optical path is η.

$$\hat{k} = \frac{1}{V}\left[2\int_0^L k_l A_l|\cos\varphi|dl + k_L A_L(W\sin\varphi - L|\cos\varphi|)\right] \tag{40}$$

$$k_l \cdot A_l = \max\left\{0, \frac{l}{\sin\varphi} - D\tan\eta\right\} \cdot D \cdot k(D,\eta) + \tan\eta \cdot \int_0^d k(h,\eta)\cdot h \cdot dh \tag{41}$$

$$d = \min\left\{D, \frac{l}{\sin\varphi\tan\eta}\right\} \tag{42}$$

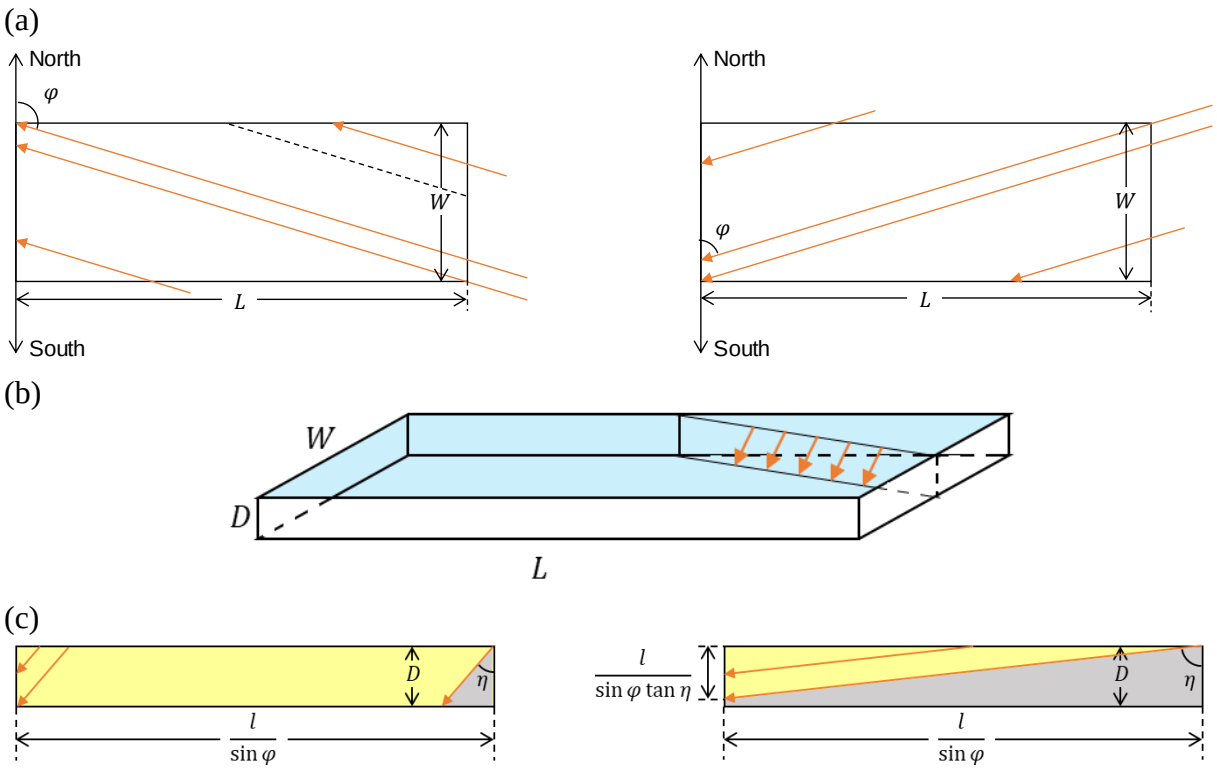

Figure 6. Sunlight irradiation through pond water when $L < W|\tan\varphi|$. Only sunlight from the east is presented. Sunlight irradiating from the west is similar. (a) top view, arrows indicate the azimuth angle of incident sunlight; (b) one vertical cross section of the pond that is parallel to incident sunlight; (c) sunlight transmission on the cross section through water body, pond bottom can be either partly illuminated or completely in shades.

Similarly, when $L > W|\tan\varphi|$ (Figure 7), $\hat{k}$ was estimated using Equations (43)-(45).

$$\hat{k} = \frac{1}{V}\left[2\int_0^W k_w A_w \sin\varphi\, dl + k_W A_W (L|\cos\varphi| - W\sin\varphi)\right] \tag{43}$$

$$k_w \cdot A_w = \max\left\{0, \frac{w}{|\cos\varphi|} - D\tan\eta\right\} \cdot D \cdot k(D,\eta) + \tan\eta \cdot \int_0^d k(h,\eta)\cdot h \cdot dh \tag{44}$$

$$d = \min\left\{D, \frac{w}{|\cos\varphi|\tan\eta}\right\} \tag{45}$$

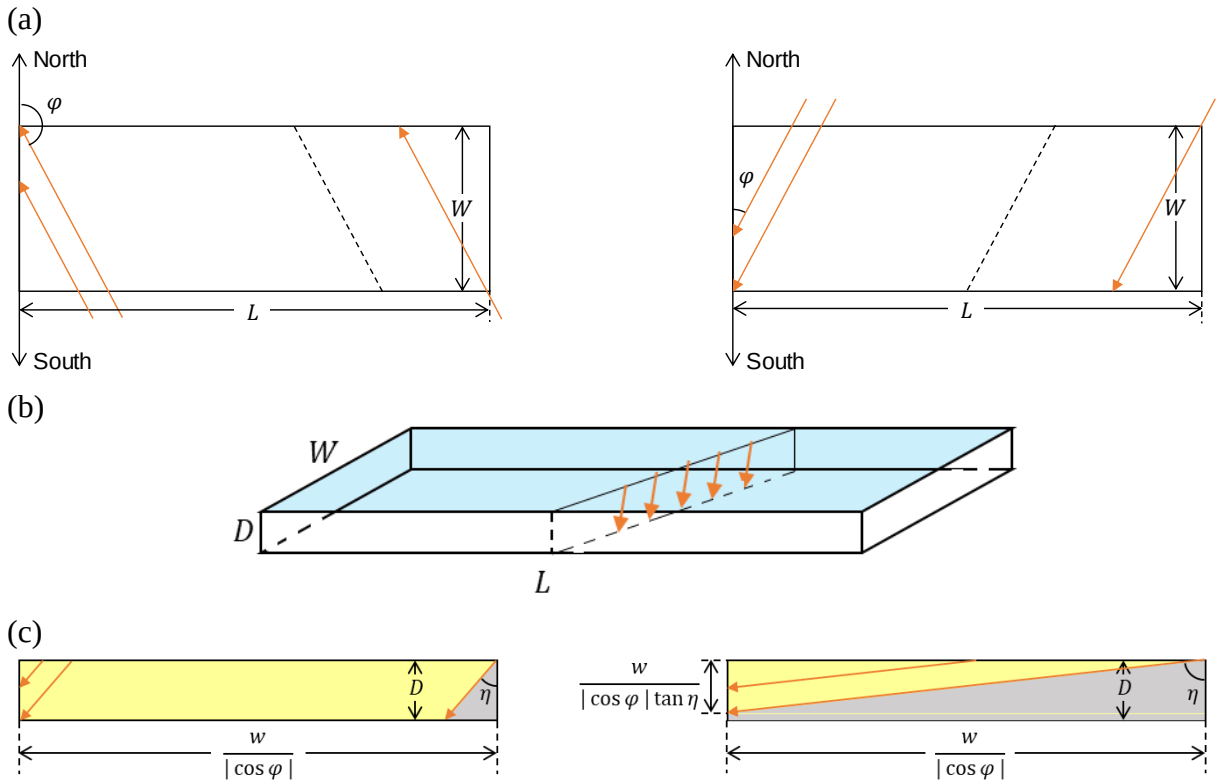

Figure 7. Sunlight irradiation through pond water when $L > W|\tan\varphi|$. Only sunlight from the east is presented. Sunlight irradiating from the west is similar. (a) top view, arrows indicate the azimuth angle of incident sunlight; (b) one vertical cross section of the pong that is parallel to incident sunlight; (c) sunlight transmission on the cross section through water body, pond bottom can be either partly illuminated or completely in shades.

To evaluate the influence of pond designs on the virus removal efficiency of the maturation pond, the median log removal of MS2 (i.e., the mean value of maximal and minimal removal within 24 hours after the system reaches equilibrium) was estimated for maturation ponds of various depths, theoretical hydraulic retention times (HRT) and length-to-width ratios. Pond depth directly affects sunlight attenuation. Length-to-width ratio has been shown to have great influence on the hydraulic performance of WSPs (Li et al., 2018). It also affects the amount of sunlight blocked by the pond walls. Given a certain sunlight irradiation condition and geometric configuration of the pond, increasing HRT of a single pond increases the virus removal rate as well as the pond volume and the required land area (Verbyla and Mihelcic, 2015b). Great efforts have also been made to study the influences of baffles and inlet and outlet settings on the hydraulic performance of WSPs (Li et al., 2018). In this study, to simplify the geometric relations between incident sunlight and reactor hydrodynamics and to minimize the

computational cost, flow patterns achieved by adding baffles can be approximated by CSTRs of a certain L/W ratio in series (von Sperling, 2007). A typical maturation pond is usually 1-1.5 m deep, with an HRT of 5-15 days (Kayombo et al., 2005). The L/W ratio of a maturation pond (Li et al., 2018) can vary from 1 to 20. As pond volume increases HRT, especially when L/W ratio is large, the hydraulic regime falls between complete mix and idealized plug flow. Therefore, simulations were run at HRT = 1, 2, 3, 4, 5 days. Pond depth was varied between 0.5 m and 1.5 m with a step size = 0.1 m, and L/W ratio = 1, 2, 4, 8, 14, 20. W/L = 2, 4, 8, 14, 20 were also simulated to represent a different orientation of the pond.

For each design, the log removal of MS2 was estimated on both the summer solstice (June 22th) and the winter solstice (December 22th) to represent the upper and lower limits of the MS2 removal rate of the maturation pond. The maturation pond was assumed to locate at 42°N, 90°W and have a constant flow rate of 10,000 $m^3 \cdot d^{-1}$. The uncertainties of photo-reactivity parameters and water quality parameters were incorporated in simulations by inputting 2048 random samples of 11 parameters for each combination of date, depth, HRT and L/W ratio. 2,703,360 simulations in total were run in Python.

3.2 Results and discussion

3.2.1 Simulated inactivation rate constants

In consistence with existing studies (Kohn et al., 2016; Love et al., 2010; Mattle et al., 2015), phiX174 was the most susceptible virus to sunlight inactivation in over 77% of the simulations, whose k_{total} [h^{-1}] had a right-tail distribution within [1.4×10^{-4}, 35] in natural water and within [2.6×10^{-4}, 35] in WSP water. KS tests on the parameters showed that small zenith angle, low NPOC concentration and small water depth tended to be more favorable for phiX174 inactivation (Table 6). Simulated k_{total} of adenovirus ranged from 8.9×10^{-5} h^{-1} to 6.2 h^{-1} in natural water and from 2.8×10^{-4} h^{-1} to 6.3 h^{-1} in WSP water (Figure 12). k_{total} of MS2 ranged from 2.2×10^{-5} h^{-1} to 1.1 h^{-1} in natural water and from 2.7×10^{-4} h^{-1} to 2.6 h^{-1} in WSP water. Depending on experimental settings such as water depth, water type and sunlight spectra, previous studies had reported k_{total} of MS2 varying from 0.149 h^{-1} to 1.2 h^{-1}, which fell in the range of the simulated results (Kohn et al., 2016; Kohn and Nelson, 2007; Love et al., 2010; Mattle et al., 2015; Nguyen et al., 2014; Silverman et al., 2015, 2013). On average, adenovirus and MS2 were much more

resistant to sunlight inactivation compared to phiX174, but they had different responses to changes of environmental and water quality parameters due to their difference in relative susceptibilities to endogenous and exogenous inactivation. Pair-wise comparison of k_{total} between viruses are shown in Figure 13. Contrast to phiX174 and adenovirus, large zenith angle, high NPOC concentration and large water depth had less negative impact on MS2 inactivation because it was more dependent on the exogenous mechanism. Noted that simulation results of adenovirus are not consistent with all previous studies. Some studies found adenovirus to be as resistant as MS2 in clear water and some natural waters (Love et al., 2010; Silverman et al., 2013). Some found it more susceptible to sunlight inactivation than MS2 in WSP water and some other natural waters (Mattle et al., 2015; Silverman et al., 2013). It is likely that some aspects of solar inactivation of adenovirus are not captured by the current model. However, there is not enough data on the $k_{virus,PPRI}$ to differentiate the distributions of $k_{virus,PPRI}$ for different water types.

In over 92% of all cases, inactivation in WSP water was faster than that in natural water for all three viruses, mainly because the absorbance spectra of WSP water tended to be more favorable for both direct photolysis and inactivation by $^1O_2$. WSP water has higher absorbance of UVA and PAR than natural water, which increases the steady-state concentration of $^1O_2$ and thus $k_{virus,^1O_2}$. On the contrary, natural water has higher absorbance of UVB so that fewer UVB photons can be absorbed by viral components to subsequently trigger direct photolysis. This effect increases with the depth of water column and causes larger difference between inactivation rates in WSP water and natural water. Detailed results of pair-wise comparison between two water types are enclosed in Appendix B.

Notwithstanding the uncertainties of multiple parameters, direct photolysis was the dominant mechanism in solar inactivation of phiX174 in almost all circumstances. Compared to 95% reported by Mattle et al. (2015), the contribution of direct photolysis ranged from 60% to 100% in natural water while when NPOC concentration in WSP water was high, the value fell in [30%, 60%] in some cases (Figure 8). The contribution of direct photolysis to k_{total} of adenovirus inactivation (varied from 2% to 100%) was over 55% in most cases. Values as low as 25% and 33% were also observed in Silverman et al.'s (2013) study. Compared to previous studies (Kohn et al., 2016; Love et al., 2010; Mattle et al., 2015; Silverman et al., 2015), the dominance of exogenous mechanisms in solar inactivation of MS2 was more significant in simulations under

varying conditions. Exogenous mechanisms contributed over 85% of k_{total} in 64.0% and 76.4% of all cases in natural water and WSP water respectively, probably because the upper bounds of $k_{\mathrm{MS2},^1\mathrm{O}_2}$ and $k_{\mathrm{MS2},^3\mathrm{CDOM}^*}$ in simulations were larger by a factor of 10 and a factor of 6 than values estimated by some studies (Kohn et al., 2016; Mattle et al., 2015), while a smaller mean value of Φ_{MS2} updated by Silverman et al. (2019) was adopted. Only in low-latitude area with abundant sunlight irradiation did endogenous mechanism play a more important role (Figure 15). $^1O_2$ was the most important reactive species in over 86% of the cases for MS2 in WSP water, but this was observed only in half the cases in natural water. Figure 9 shows that NPOC concentration was correlated with the relative contributions of different reactive species. In APEX model, unlike ^{3}CDOM* or $^1O_2$, $^\bullet$OH can also be produced from NO_3^- and NO_2^- besides CDOM, which is closely related to NPOC, and $^\bullet$OH itself as well as ^{3}CDOM* are both sources of $CO_3^{\bullet-}$. As a result, the steady-state concentrations of ^{3}CDOM* and $^1O_2$ are more sensitive to changes of NPOC concentration. When NPOC concentration was below 10 mg-C·L^{-1}, multiple-source species ($^\bullet$OH and $CO_3^{\bullet-}$) tended to have a larger contribution to overall inactivation than single-source species, which may explain why observed $k_{virus,^1\mathrm{O}_2}$ varies across different water types when $^1O_2$ was used as the single indicator of exogenous inactivation (Silverman et al., 2019a).

Table 2. Mean values of simulated pseudo 1st-order inactivation rate constants in Morris analysis (unit: h^{-1}). The coefficients of variation are reported in parentheses.

	Mechanism	Adenovirus	MS2	PhiX174
Natural water	Photolysis	1.24×10^{-1} (3.34)	1.41×10^{-2} (3.51)	7.73×10^{-1} (3.29)
	$^\bullet$OH	1.76×10^{-3} (2.08)	3.11×10^{-3} (2.07)	7.12×10^{-4} (2.11)
	$CO_3^{\bullet-}$	3.27×10^{-3} (4.71)	5.30×10^{-3} (4.64)	2.46×10^{-3} (4.79)
	$^1O_2$	2.10×10^{-3} (1.84)	1.00×10^{-2} (2.15)	5.53×10^{-4} (1.85)
	^{3}CDOM*	3.41×10^{-4} (1.96)	8.86×10^{-3} (2.15)	8.28×10^{-5} (1.91)
	Total	1.31×10^{-1} (3.23)	4.14×10^{-2} (2.16)	7.77×10^{-1} (3.29)
WSP water	Photolysis	1.39×10^{-1} (3.11)	1.58×10^{-2} (3.26)	8.70×10^{-1} (3.07)
	$^\bullet$OH	2.14×10^{-3} (1.87)	3.78×10^{-3} (1.86)	8.64×10^{-4} (1.90)
	$CO_3^{\bullet-}$	9.03×10^{-6} (4.43)	1.46×10^{-5} (4.36)	6.78×10^{-6} (4.50)
	$^1O_2$	1.13×10^{-2} (1.74)	5.43×10^{-2} (2.03)	2.99×10^{-3} (1.74)
	^{3}CDOM*	4.50×10^{-4} (1.84)	1.17×10^{-2} (2.02)	1.09×10^{-4} (1.79)
	Total	1.53×10^{-1} (2.91)	8.56×10^{-2} (1.91)	8.74×10^{-1} (3.06)

Regardless of water type or virus species, a considerable uncertainty of output inactivation rate constants was observed due to the simultaneous variation of a series of parameters (Table 2). In comparison, the k_{total} of adenovirus and phiX174 had larger coefficients of variation, which

were mainly introduced by the uncertainty of the k_{endo}. Since endogenous inactivation is directly determined by the photon flux density of sunlight and the attenuation along the optical path in water, k_{endo} tended to be more sensitive than k_{exo} to the variations of environmental and water quality parameters.

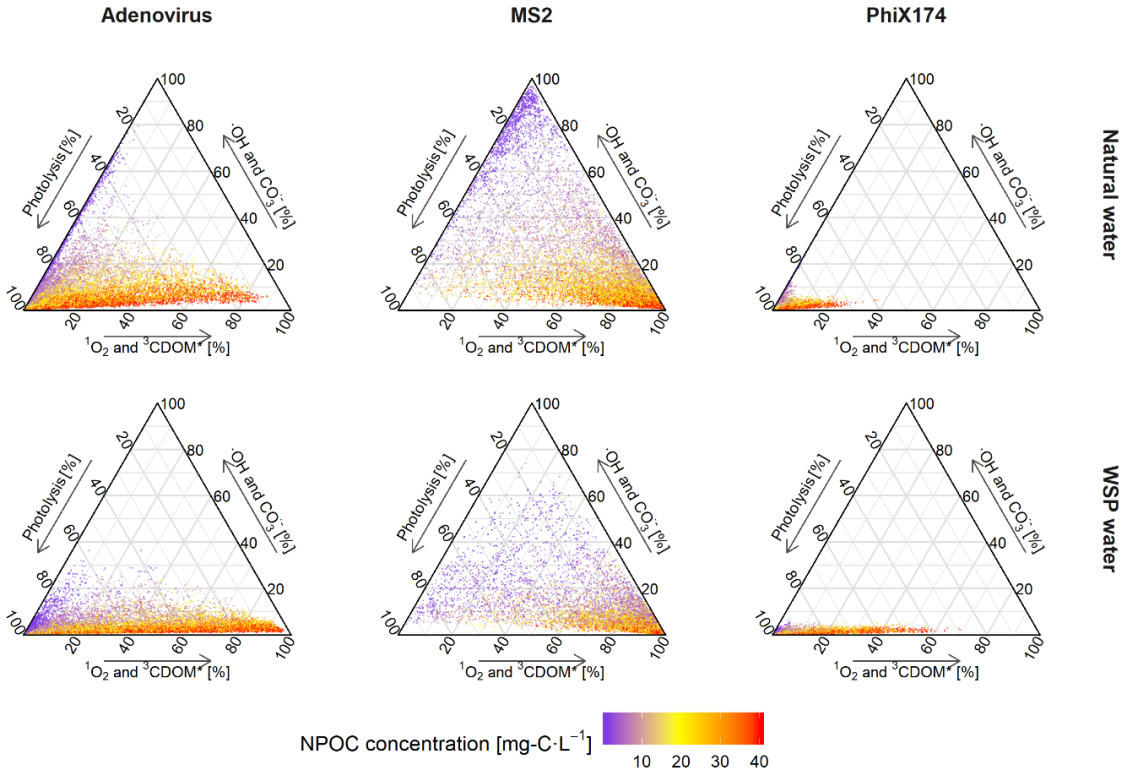

Figure 8. Ternary plot of contributions of inactivation by different mechanisms vs. NPOC concentration in simulation. $^3CDOM^*$ and $^1O_2$ were grouped as single-source reactive species. $^\bullet OH$ and $CO_3^{\bullet-}$ were grouped as multiple-source reactive species.

3.2.2 Relative importance of input parameters to the total inactivation rate constant

Among the 17 parameters in Morris analysis, time relative to sunrise and sunset, depth of the water column and latitude stood out to be the most relevant parameters to k_{total} regardless of virus species or water type. They also had the largest σ, meaning that they had the strongest interactions with other parameters. Second to these parameters were month and the concentration NPOC for all virus-water combinations. Latitude, season and local time together determined the spectrum and the zenith angle of incident sunlight. The incident angle and water depth determined the length of the optical path, and thus, the attenuation of sunlight. The concentration of NPOC, as the major photosensitizer in water, affects not only the steady-state concentrations

of reactive species but also k_{endo} by competing with viral components in absorbing sunlight photons. Because direct photolysis was the major inactivation mechanism despite the uncertainties of photo-reactivity parameters, the k_{total} of adenovirus and phiX174 had also had relatively high sensitivity to the scale factor of the molar absorption coefficients (ε_{virus}), which directly determined the level of photon absorption by viral components and thus the magnitude of direct photolysis. The k_{total} of MS2 in WSP water, on the contrary, was more sensitive to the shape factor of water absorbance spectrum (β) and the 2nd-order inactivation rate constant by $^1O_2$ ($k_{virus,^1O_2}$). Other environmental parameters (longitude and altitude), water quality parameters (α, [NO_3^-] and [NO_2^-]) and most photo-reactivity parameters had relatively small impacts on k_{total}. However, since cloud cover was not taken into consideration in sunlight irradiance modeling, the importance of altitude may have been underestimated. The σ/μ^* ratio of all parameters varied in the model were larger than 1, indicating the non-linear structure of the integrated solar virus inactivation model. Therefore, Sobol' method was a valid choice for a robust sensitivity analysis of the model.

In general, results of Morris and Sobol' analyses agreed well with each other. For all virus species and water types, the largest value of main effect S_i was obtained for water depth (25.9~36.5%), followed by time relative to sunrise and sunset (10.2~18.9%), NPOC concentration (4.6~6.3%) and location (1.9~2.4%). Specific to k_{total} of MS2 inactivation in WSP water, the main effect of $k_{virus,^1O_2}$ was 6.4%, exceeding those of location and NPOC concentration. Consistent with results of Morris analysis, the scale factor of ε_{virus} had an S_i over 1% only for adenovirus and phiX174, while β's S_i was larger than 1% for both MS2 and phiX174 in WSP water. The importance of location was less significant in Sobol' analysis than in Morris analysis. However, the result of Sobol' analysis was more accurate since location was sampled from empirical land-area elevation dataset. The main effects of all parameters added up to 65% for MS2, but this value was less than 50% for adenovirus and phiX174 in both water types, meaning that interactions among parameters played a significant role in the uncertainty of k_{total}, and a global method of sensitivity analysis is essential.

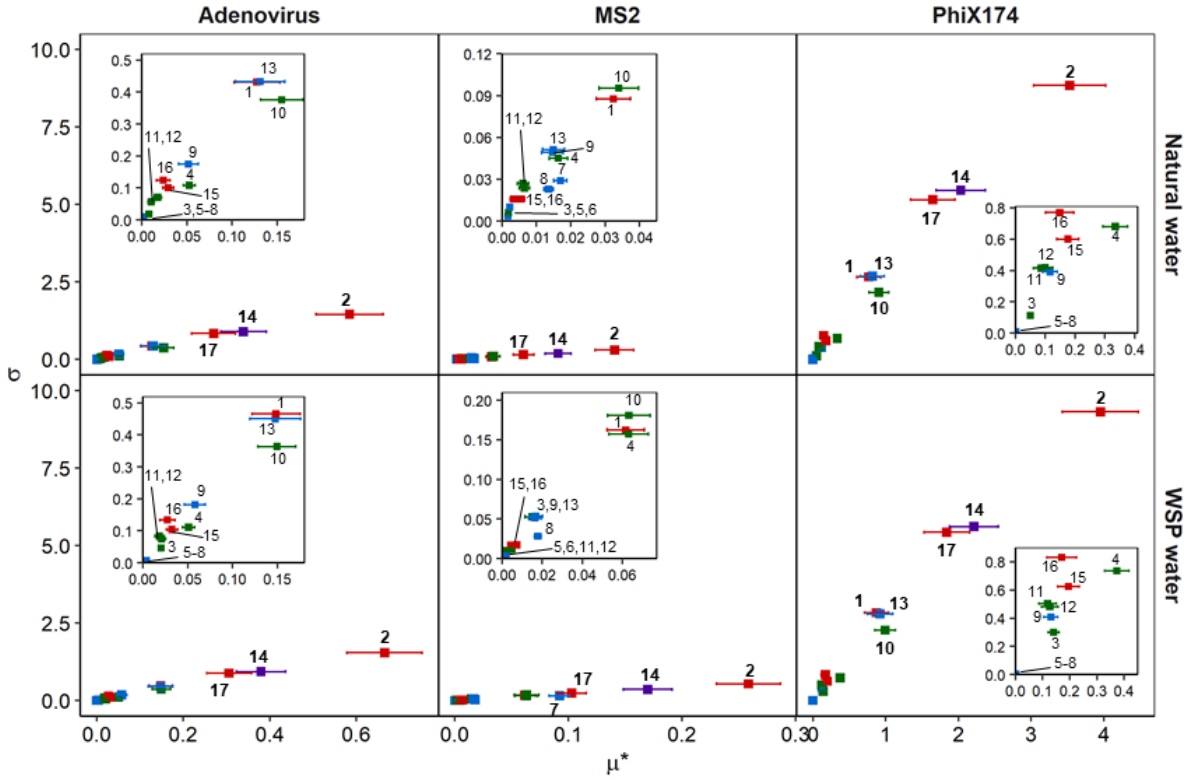

Figure 9. Morris sensitivity indices of k_{total} against 17 parameters. Red points represent environmental parameters: 1 – month, 2 – time, 15 – altitude, 16 – longitude, 17 – latitude; Blue points are photo-reactivity parameters: 5 – $k_{virus,\cdot OH}$, 6 – $k_{virus,CO_3^{\cdot-}}$, 7 – $k_{virus,^1O_2}$, 8 – $k_{virus,^3CDOM^*}$, 9 – Φ_{virus}, 13 – ε_{virus}; Green points are water quality parameters: 3 – α, 4 – β, 10 – [NPOC], 11 – [NO_3^-], 12 – [NO_2^-]; The engineering design parameter, 14 – water depth, is in purple. Whiskers indicate the 95% confidence intervals of μ^*.

As is shown in Figure 10, 75-83% of the variance of k_{total} was driven by the main effects and 2nd-order interaction effects between 8 parameters, among which the S_{im} between water depth and time, NPOC concentration or location accounted for a considerable proportion, particularly for phiX174 and adenovirus whose inactivation was dominated by endogenous mechanism. In total, eliminating the uncertainty of water depth can reduce the variance of k_{total} by 64.1~75.0% depending on virus species and water type (Table 10). Fixing location alone can also reduce the uncertainty of k_{total} by 11.8~24.9%. Nevertheless, for a certain treatment system, e.g., a maturation pond that operates continuously on 24-hour cycles at a certain location, the variance of k_{total} introduced by water quality fluctuations as well as diurnal and seasonal changes cannot be eliminated. As a result, the uncertainties of most photo-reactivity parameters remain irrelevant. The only exception would be the $k_{virus,^1O_2}$ for MS2 in WSP water and ε_{virus} for adenovirus and phiX174, whose S_{Ti} were 16.8%, 8.3~8.7% and 8.9~9.3%

respectively. In summary, engineering design and environmental parameters had greater influence on the k_{total} of virus inactivation than photo-reactivity or water quality parameters.

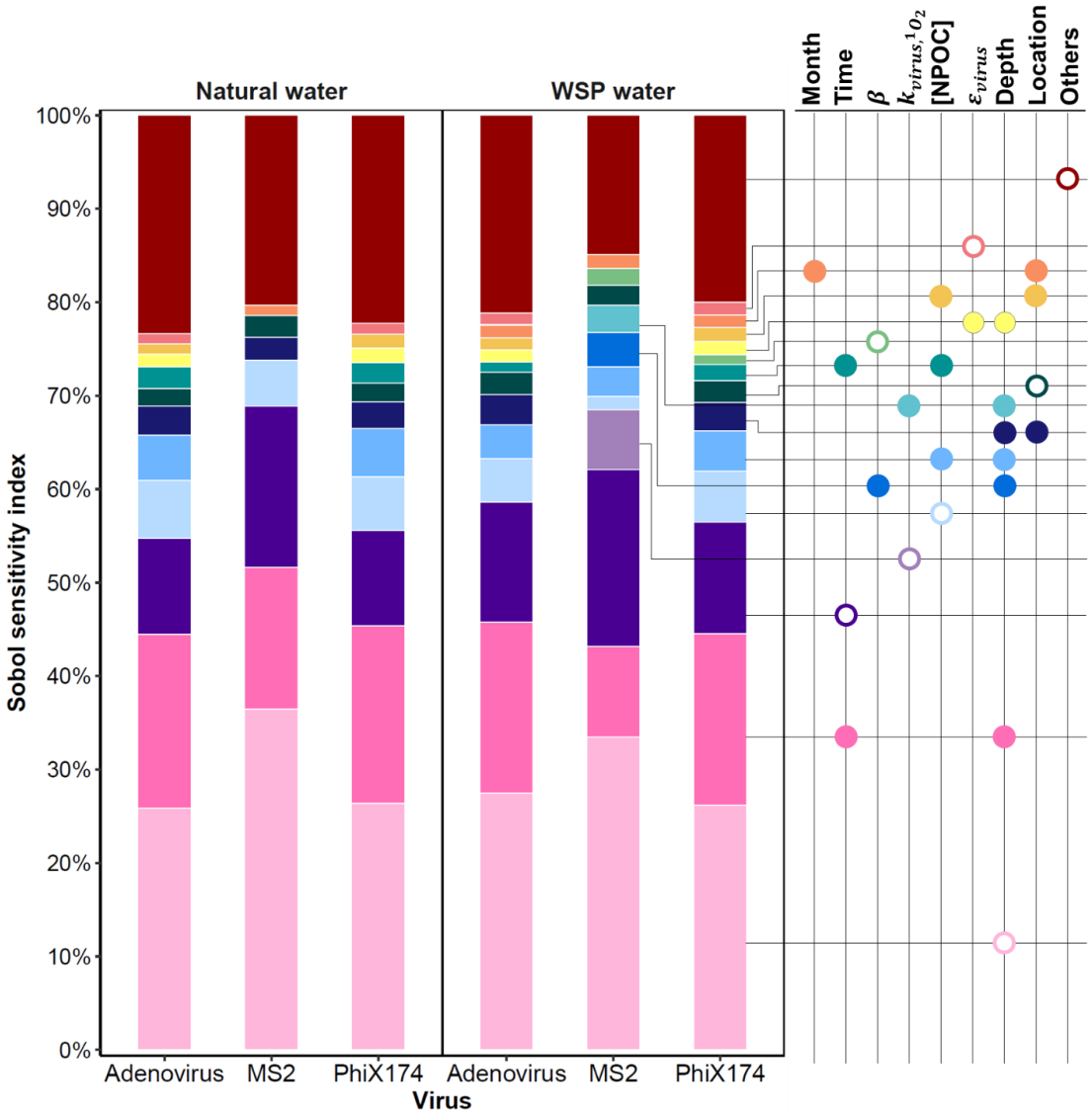

Figure 10. Decomposition of the variance of k_{total} into variances introduced by different parameters. Filled dots represent interaction effects (S_{im}) between two parameters. Hollow dots indicate main effects (S_i) of individual parameters. Only sensitivity indices larger than 1% are presented. Other parameters include α, $k_{virus,\cdot OH}$, $k_{virus,CO_3^{\cdot-}}$, $k_{virus,^3CDOM^*}$, Φ_{virus}, [NO_3^-] and [NO_2^-].

3.2.3 Influence of maturation pond design on MS2 removal efficiency

To quantify the uncertainty of the virus removal efficiency of a treatment system utilizing sunlight-mediated inactivation and illustrate the influence of engineering designs, the log removal of MS2 was predicted for each design described above. As shown in Figure 11, the uncertainty of

log removal induced by the variations of water quality and photo-reactivity parameters was considerable regardless of design. For maturation pond system that has a total HRT of 5 days and a constant depth of 1.5 m, the log removal of MS2 can reach 0.25~2.30 on summer solstice and 0.06~0.84 on winter solstice.

Pair-wise comparison of different pond configurations (Figure 11a) showed that, given the first-order kinetics of solar virus inactivation, reducing the level of mixing can always improve the virus removal efficiency of the system during daytime. This effect scales with the original log removal, resulting in a larger total variance of log removal in a less-mix system than a CSTR under fluctuating water quality conditions. In other words, if the water quality was unfavorable, improvement of log removal by reducing mixing would also be very limited. However, a less-mix system will experience larger diurnal fluctuations of effluent quality due to the complete shut-down of solar inactivation during nighttime. Among the design parameters examined, length-to-width ratio of the complete-mix pond had negligible influence on general sunlight exposure and the log removal at equilibrium. Although depth was shown to be the most important parameter for k_{total} in sensitivity analyses, the improvement of log removal by reducing pond depth from 1.5 m to 0.5 m was below 0.4 but with a 200% increase in required pond area. Adding maturation ponds in series was a more efficient design to improve log removal. Increasing HRT to 10 days by adding 5 identical maturation ponds in series can improve the log removal of MS2 by 1.5 on average on summer solstice while only results in a 100% increase of total pond area. Seasonal change significantly impacted the virus removal system. A system of 10 identical maturation ponds (HRT = 1 day, depth = 0.5 m) in series could provide 2-log removal of MS2 at maximum in winter if it could still operate. The location (42°N, 90°W) was the major limitation to the MS2 removal performance.

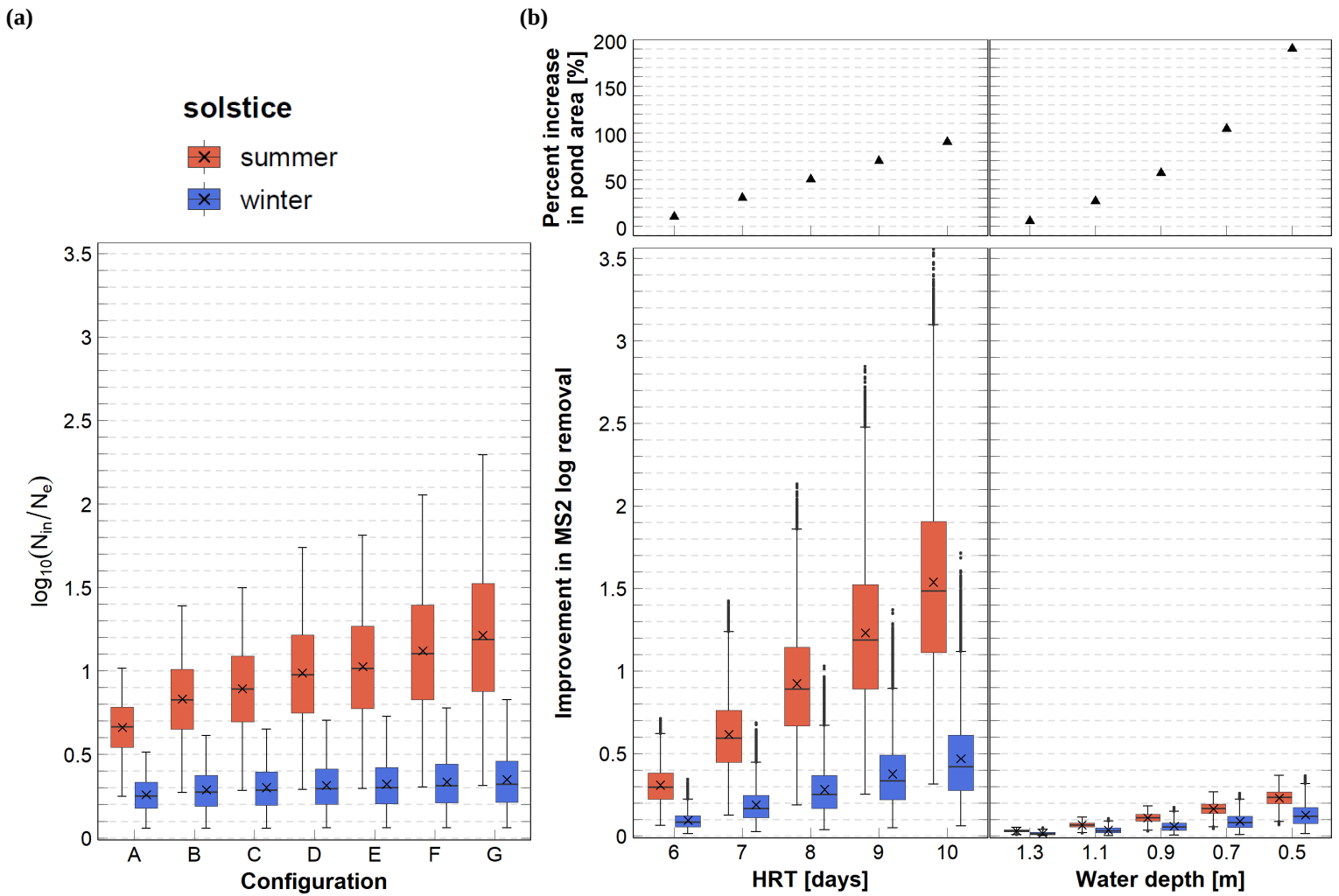

Figure 11. Simulated average MS2 log removal of maturation pond system of various designs. (a) baseline scenario (HRT = 5 days, depth = 1.5 m). MS2 log removal depends on the configuration the system: A. single pond, HRT [d] = 5; B. two ponds in series, HRT [d] = 4 + 1; C. two ponds in series, HRT [d] = 3 + 2; D. three ponds in series, HRT [d] = 3 + 1 + 1; E. three ponds in series, HRT [d] = 2 + 2 + 1; F. four ponds in series, HRT [d] = 2 + 1 + 1 + 1; G. five ponds in series, HRT [d] = 1×5. (b) increase in MS2 log removal and pond area by reducing pond depth or increasing the number of maturation ponds (HRT = 1 day) in series from baseline scenario.

CHAPTER 4: CONCLUSIONS AND ENGINEERING SIGNIFICANCE

As a widely applied disinfection mechanism for low-cost water and wastewater treatment, solar virus inactivation has been better understood in the past few years. Yet the virus removal efficiency of these treatment systems is subject to high uncertainty. To facilitate accurate prediction of solar virus inactivation rate and to provide information for the engineering design of reliable and efficient treatment systems for virus removal, this study investigated different sources of uncertainty and elucidated the relative importance of different factors for solar virus inactivation through global sensitivity analyses of a mechanistic model. By adapting and combining the aquatic photochemistry model APEX with the existing sunlight spectrum model SMARTS, the study enclosed independent environmental factors, photo-reactivity factors, water quality factors and design factors in one mathematical framework. Monte Carlo simulations of the integrated model on three virus and two water types were run across the whole variation space of the factors to characterize the uncertainty of solar virus inactivation. Morris OAT screening and Sobol' variance-based sensitivity analysis were performed to compare and quantify the relative importance of the factors. A 3-D CSTR model coupled with the integrated solar virus inactivation model was developed to further reveal the influence of design factors on the virus removal performance of a maturation pond system.

The modeled pseudo first-order inactivation rate constants responded to variations of different factors in a consistent manner with previous understanding of the inactivation mechanisms. Simultaneous variations of 15 factors invariably induced a considerable amount of uncertainty in the prediction of total inactivation rate for all virus species and both water types. Some values of simulated k_{total} seemed extremely high given the limited diffusivity of water constituents, suggesting that the current solar virus inactivation model needs further verification and calibration under extreme conditions. Since environmental, water quality and design parameters become certain upon measurement, to improve the accuracy and reliability of the solar virus inactivation model, it is essential to reduce the uncertainty of photo-reactivity parameters through rigorous experiments with controlled conditions.

Simultaneous variation of different factors allowed some simulations to output results that were not observed in previous experimental studies. MS2 was less resistant than phiX174 or adenovirus in some cases, because the relative susceptibility to endogenous and exogenous

inactivation varies among virus species. And endogenous inactivation is more sensitive to changes of sunlight exposure (i.e., location, time, water depth and water absorbance) than exogenous mechanism. Using MS2 as the single surrogate of solar virus inactivation may cause overestimation of the virus removal performance of a treatment system under certain conditions, such as high NPOC concentration and low sunlight exposure. $^1O_2$ was not always the most important PPRI for exogenous inactivation, either. In some circumstances, e.g., when NPOC concentration is low while nitrate and nitrite are relatively abundant, inactivation by $^\bullet OH$ and $CO_3^{\bullet-}$ tends to be more significant, because the formation of $^1O_2$ is sensitized by ^{3}CDOM* that is produced only from NPOC while nitrate and nitrite in water can also sensitize the formation of $^\bullet OH$ and $CO_3^{\bullet-}$ upon absorption of sunlight. Therefore, $^1O_2$ is not a valid surrogate for exogenous inactivation for every virus species or every physicochemical condition of water. Estimation of $k_{virus,^1O_2}$ based on such modeling strategy is likely biased. Contributions of other PPRIs to exogenous inactivation of virus are not negligible. Including all relevant PPRIs in the modeling of solar virus inactivation is necessary for more accurate and robust prediction.

Both global sensitivity analyses showed that environmental and engineering design parameters significantly outweigh water quality and photo-reactivity parameters in the determination of virus inactivation rate constants. Interaction effects among different parameters were shown to have important contributions to the variance of k_{total}, implying the complexity of the solar virus inactivation processes. Main effects of 15 factors took up 50~65% of total variance, which were heavily concentrated on only a few parameters. Sunlight, especially UVB, is mostly attenuated by water constituents in the first 30 cm of the optical path. As a result, variation of water depth between 0.01 m and 3 m is the most important single source of uncertainty, accounting for 25.9~36.5% of the variance of k_{total}, while reducing pond depth from 1.5 m to 0.5 m brought less effective improvement of the virus removal efficiency of a maturation pond. Diurnal motion of the sun is the second most influential factor for solar virus inactivation, followed by location and NPOC concentration of the water. When the variations of environmental, water quality or design parameters exist, variance of k_{total} resulting from the uncertainties of photo-reactivity parameters remains irrelevant. For a certain treatment system, the virus removal potential is determined by the location and engineering design, but the virus removal efficiency is inevitably influenced by the diurnal and seasonal solar motions as well as

the fluctuation of water quality. Since the temporal variations of water quality and sunlight irradiance cannot be eliminated, the uncertainties of photo-reactivity parameters would not introduce significant error to the estimation of virus inactivation rate. The virus removal efficiency of a treatment system can be improved or optimized through informed design.

Monte Carlo simulation results of MS2 log removal of different designs for a maturation pond system showed that increasing hydraulic efficiency and HRT should be prioritized over reducing pond depth to effectively improve the virus removal efficiency of the maturation pond at minimal costs. Common strategies to improve the hydraulic efficiency of a pond system, such as increasing length-to-width ratio and adding baffles, do not significantly impact the solar virus inactivation rates of the system, although they tend to partly reduce the exposure of water body to sunlight irradiance. CSTRs in series can achieve much better removal performance than single CSTR, but effluent quality would also be more fluctuant due to a complete shut-down of solar inactivation during nighttime and less mixing. The interaction effect between short-circuiting and sunlight blockage is not capture by this model.

Based on the findings of this work, several further research needs are identified. More accurate modeling of UVB irradiance on water surface is needed to improve the prediction of k_{total}, especially for virus species dominant by endogenous mechanism. To enable the prediction of solar virus inactivation across various water conditions, common indicators of physicochemical conditions including pH, DO and temperature should be incorporated into the photochemistry model. Quantitative understandings of interaction between algae growth and solar virus inactivation is also in need to characterize the process in algae-rich water bodies (e.g. high-rate algae pond). This study performed Monte Carlo simulations on a simple CSTR model and gained insights on the influence of different design factors on the solar virus removal performance for a maturation pond system. However, for precise optimization of pond design, a more sophisticated solar virus inactivation model capturing the geometry relation between sunlight exposure and hydrodynamics of the system is needed.

REFERENCES

Amarasiri, M., Kitajima, M., Nguyen, T.H., Okabe, S., 2017. Bacteriophage removal efficiency as a validation and operational monitoring tool for virus reduction in wastewater reclamation : Review. Water Res. 121, 258–269. https://doi.org/10.1016/j.watres.2017.05.035

Apell, J.N., McNeill, K., 2019. Updated and validated solar irradiance reference spectra for estimating environmental photodegradation rates. Environ. Sci. Process. Impacts 21, 427–437. https://doi.org/10.1039/c8em00478a

Badrot-Nico, F., Guinot, V., Brissaud, F., 2009. Fluid flow pattern and water residence time in waste stabilisation ponds. Water Sci. Technol. 59, 1061–1068. https://doi.org/10.2166/wst.2009.087

Bodrato, M., Vione, D., 2014. APEX (Aqueous Photochemistry of Environmentally occurring Xenobiotics): a free software tool to predict the kinetics of photochemical processes in surface waters. Environ. Sci. Process. Impacts 16, 732–740. https://doi.org/10.1039/C3EM00541K

Boehm, A.B., Yamahara, K.M., Love, D.C., Peterson, B.M., Mcneill, K., Nelson, K.L., 2009. Covariation and photoinactivation of traditional and novel indicator organisms and human viruses at a sewage-impacted marine beach. Environ. Sci. Technol. 43, 8046–8052. https://doi.org/10.1021/es9015124

Bolton, N.F., Cromar, N.J., Hallsworth, P., Fallowfield, H.J., 2010. A review of the factors affecting sunlight inactivation of micro-organisms in waste stabilisation ponds : preliminary results for enterococci. Water Sci. Technol. 885–890. https://doi.org/10.2166/wst.2010.958

Bosshard, F., Armand, F., Hamelin, R., Kohn, T., 2013. Mechanisms of human adenovirus inactivation by sunlight and UVC light as examined by quantitative PCR and quantitative proteomics. Appl. Environ. Microbiol. 79, 1325–1332. https://doi.org/10.1128/AEM.03457-12

Campolongo, F., Cariboni, J., Saltelli, A., 2007. An effective screening design for sensitivity analysis of large models. Environ. Model. Softw. 22, 1509–1518. https://doi.org/10.1016/j.envsoft.2006.10.004

Cariboni, J., Gatelli, D., Liska, R., Saltelli, A., 2007. The role of sensitivity analysis in ecological modelling. Ecol. Modell. 203, 167–182. https://doi.org/10.1016/j.ecolmodel.2005.10.045

Carratalà, A., Calado, A.D., Mattle, M.J., Meierhofer, R., Luzi, S., Kohn, T., 2016. Solar disinfection of viruses in polyethylene terephthalate bottles. Appl. Environ. Microbiol. 82, 279–288. https://doi.org/10.1128/AEM.02897-15

Curtis, T.P., Mara, D.D., Dixo, N.G.H., Silva, S.A., 1994. Light penetration in waste stabilization ponds. Water Res. 28, 1030–1038.

Dahl, N.W., Wood, P.L., Lemckert, C.J., Stratton, H., Roiko, A., 2017. A practical model for sunlight disinfection of a subtropical maturation pond. Water Res. 108, 151–159. https://doi.org/10.1016/j.watres.2016.10.072

Davies-Colley, R.J., 2005. Pond Disinfection, in: Shilton, A. (Ed.), Pond Treatment Technology. IWA Publishing, London, pp. 100–136. https://doi.org/10.2166/9781780402499

Davies-Colley, R.J., Donnison, A.M., Speed, D.J., 2000. Towards a mechanistic understanding of pond disinfection. Water Sci. Technol. 42, 149–158.

Davies-Colley, R.J., Donnison, A.M., Speed, D.J., Ross, C.M., Nagels, J.W., 1999. Inactivation of faecal indicator microorganisms in waste stabilisation ponds: interactions of environmental factors with sunlight. Water Res. 33, 1220–1230.

De Laurentiis, E., Minella, M., Bodrato, M., Maurino, V., Minero, C., Vione, D., 2013. Modelling the photochemical generation kinetics of 2-methyl-4-chlorophenol, an intermediate of the herbicide MCPA (2-methyl-4-chlorophenoxyacetic acid) in surface waters. Aquat. Ecosyst. Heal. Manag. 16, 216–221. https://doi.org/10.1080/14634988.2013.788433

Dias, D.F.C., Passos, R.G., von Sperling, M., 2017. A review of bacterial indicator disinfection mechanisms in waste stabilisation ponds. Rev. Environ. Sci. Biotechnol. 16, 517–539. https://doi.org/10.1007/s11157-017-9433-2

Dias, D.F.C., Von Sperling, M., 2017. Solar radiation (PAR, UV-A, UV-B) penetration in a shallow maturation pond operating in a tropical climate. Water Sci. Technol. 76, 182–191. https://doi.org/10.2166/wst.2017.203

Fisher, M.B., Love, D.C., Schuech, R., Nelson, K.L., 2011. Simulated sunlight action spectra for inactivation of MS2 and PRD1 bacteriophages in clear water. Environ. Sci. Technol. 45, 9249–9255. https://doi.org/10.1021/es201875x

Gan, Y., Duan, Q., Gong, W., Tong, C., Sun, Y., Chu, W., Ye, A., Miao, C., Di, Z., 2014. A comprehensive evaluation of various sensitivity analysis methods: A case study with a hydrological model. Environ. Model. Softw. 51, 269–285. https://doi.org/10.1016/j.envsoft.2013.09.031

Gueymard, C.A., 1995. SMARTS2: a simple model of the atmospheric radiative transfer of sunshine: algorithms and performance assessment. Cocoa, FL. https://doi.org/FSEC-PF-270-95

Herman, J., Usher, W., 2017. SALib : An open-source Python library for Sensitivity Analysis. J. Open Source Softw. 41, 9–10. https://doi.org/10.1016/S0010-1

Iooss, B., Lemaitre, P., 2015. A review on global sensitivity analysis methods, in: Meloni, C., Dellino, G. (Eds.), Uncertainty Management in Simulation-Optimization of Complex Systems: Algorithms and Applications. Springer, pp. 1–24.

Jarvis, A., Reuter, H.I., Nelson, A., Guevara, E., 2008. Hole-filled SRTM for the globe Version 4 [WWW Document]. CGIAR-CSI SRTM 90m Database. URL https://cgiarcsi.community/data/srtm-90m-digital-elevation-database-v4-1/ (accessed 3.4.18).

Kayombo, S., Mbwette, T.S.A., Katima, J.H.Y., Ladegaard, N., Jørgensen, S.E., 2005. Waste stabilization ponds and constructed wetlands: design manual, UNEP-IETC with the Danish International Development Agency.

Kohn, T., Grandbois, M., Mcneill, K., Nelson, K.L., 2007. Association with natural organic matter enhances the sunlight-mediated inactivation of MS2 coliphage by singlet oxygen. Environ. Sci. Technol. 41, 4626–4632. https://doi.org/10.1021/es070295h

Kohn, T., Mattle, M.J., Minella, M., Vione, D., 2016. A modeling approach to estimate the solar disinfection of viral indicator organisms in waste stabilization ponds and surface waters. Water Res. 88, 912–922. https://doi.org/10.1016/j.watres.2015.11.022

Kohn, T., Nelson, K.L., 2007. Sunlight-mediated inactivation of MS2 coliphage via exogenous singlet oxygen produced by sensitizers in natural waters. Environ. Sci. Technol. 41, 192–197. https://doi.org/10.1021/es061716i

Li, M., Zhang, H., Lemckert, C., Roiko, A., Stratton, H., 2018. On the hydrodynamics and treatment efficiency of waste stabilisation ponds : From a literature review to a strategic evaluation framework. J. Clean. Prod. 183, 495–514. https://doi.org/10.1016/j.jclepro.2018.01.199

Liu, L., Hall, G., Champagne, P., 2016. Effects of Environmental Factors on the Disinfection Performance of a Wastewater Stabilization Pond Operated in a Temperate Climate. Water 8, 1–11. https://doi.org/10.3390/w8010005

Love, D.C., Silverman, A., Nelson, K.L., 2010. Human virus and bacteriophage inactivation in clear water by simulated sunlight compared to bacteriophage inactivation at a Southern California beach. Environ. Sci. Technol. 44, 6965–6970. https://doi.org/10.1021/es1001924

Maiga, Y., Wethe, J., Denyigba, K., Ouattara, A.S., 2009. The impact of pond depth and environmental conditions on sunlight inactivation of Escherichia coli and enterococci in wastewater in a warm climate. Can. J. Microbiol. 55, 1364–1374. https://doi.org/10.1139/W09-104

Mamane, H., Shemer, H., Linden, K.G., 2007. Inactivation of E. coli, B. subtilis spores, and MS2, T4, and T7 phage using UV/H2O2 advanced oxidation. J. Hazard. Mater. 146, 479–486. https://doi.org/10.1016/j.jhazmat.2007.04.050

Mattle, M.J., Vione, D., Kohn, T., 2015. Conceptual model and experimental framework to determine the contributions of direct and indirect photoreactions to the solar disinfection of MS2, phiX174, and adenovirus. Environ. Sci. Technol. 49, 334–342. https://doi.org/10.1021/es504764u

McGuigan, K.G., Conroy, R.M., Mosler, H.J., du Preez, M., Ubomba-Jaswa, E., Fernandez-Ibañez, P., 2012. Solar water disinfection (SODIS): A review from bench-top to roof-top. J. Hazard. Mater. 235–236, 29–46. https://doi.org/10.1016/j.jhazmat.2012.07.053

McKay, M.D., Morrison, J.D., Upton, S.C., 1999. Evaluating prediction uncertainty in simulation models. Comput. Phys. Commun. 117, 44–51. https://doi.org/10.1016/S0010-4655(98)00155-6

Morris, M.D., 1991. Factorial plans for preliminary computational experiments. Technometrics 33, 161–174.

Nelson, K.L., Boehm, A.B., Davies-colley, R.J., Dodd, M.C., Kohn, T., Linden, K.G., Liu, Y., Maraccini, P.A., Mcneill, K., Mitch, W.A., Nguyen, T.H., Parker, K.M., Rodriguez, R.A.,

Sassoubre, L.M., Silverman, A.I., Wigginton, R., Zepp, R.G., 2018. Sunlight-mediated inactivation of health-relevant microorganisms in water: a review of mechanisms and modeling approaches. Environ. Sci. Process. Impacts 20, 1089–1122. https://doi.org/10.1039/c8em00047f

Nguyen, M.T., Silverman, A.I., Nelson, K.L., 2014. Sunlight inactivation of ms2 coliphage in the absence of photosensitizers: Modeling the endogenous inactivation rate using a photoaction spectrum. Environ. Sci. Technol. 48, 3891–3898. https://doi.org/10.1021/es405323p

Noyola, A., Padilla-Rivera, A., Morgan-Sagastume, J.M., Güereca, L.P., Hernández-Padilla, F., 2012. Typology of Municipal Wastewater Treatment Technologies in Latin America. Clean - Soil, Air, Water 40, 926–932. https://doi.org/10.1002/clen.201100707

Oliveira, S.C., von Sperling, M., 2011. Performance evaluation of different wastewater treatment technologies operating in a developing country. J. Water, Sanit. Hyg. Dev. 1, 37–56. https://doi.org/10.2166/washdev.2011.022

Ouali, A., Jupsin, H., Vasel, J.L., Ghrabi, A., 2015. Removal of E . coli and enterococci in maturation pond and kinetic modelling under sunlight conditions. Desalin. Water Treat. 54, 1068–1074. https://doi.org/10.1080/19443994.2013.856350

Romero-Maraccini, O.C., Sadik, N.J., Rosado-Lausell, S.L., Pugh, C.R., Niu, X.Z., Croué, J.P., Nguyen, T.H., 2013. Sunlight-induced inactivation of human Wa and porcine OSU rotaviruses in the presence of exogenous photosensitizers. Environ. Sci. Technol. 47, 11004–11012. https://doi.org/10.1021/es402285u

Romero, O.C., Straub, A.P., Kohn, T., Nguyen, T.H., 2011. Role of temperature and suwannee river natural organic matter on inactivation kinetics of rotavirus and bacteriophage MS2 by solar irradiation. Environ. Sci. Technol. 45, 10385–10393. https://doi.org/10.1021/es202067f

Rosado-Lausell, S.L., Wang, H., Gutiérrez, L., Romero-Maraccini, O.C., Niu, X.Z., Gin, K.Y.H., Croué, J.P., Nguyen, T.H., 2013. Roles of singlet oxygen and triplet excited state of dissolved organic matter formed by different organic matters in bacteriophage MS2 inactivation. Water Res. 47, 4869–4879. https://doi.org/10.1016/j.watres.2013.05.018

Saltelli, A., 2002. Sensitivity analysis for importance assessment. Risk Anal. 22, 579–590. https://doi.org/10.1002/0470870958.ch2

Saltelli, A., Tarantola, S., Campolongo, F., Ratto, M., 2004. Sensitivity Analysis in Practice: A Guide to Assessing Scientific Models. John Wiley & Sons Ltd, Chichester.

Saltelli, A., Tarantola, S., Chan, K.P.S., 1999. A Quantitative Model-Independent Method for Global Sensitivity Analysis of Model Output. Technometrics 41, 39–56.

Silverman, A.I., Nguyen, M.T., Jasper, J.T., Boehm, A.B., Nelson, K.L., 2015. Sunlight inactivation of fecal indicator bacteria in open-water unit process treatment wetlands: Modeling endogenous and exogenous inactivation rates. Environ. Sci. Technol. 49, 2757–2766. https://doi.org/10.1021/es5049754

Silverman, A.I., Peterson, B.M., Boehm, A.B., McNeill, K., Nelson, K.L., 2013. Sunlight inactivation of human viruses and bacteriophages in coastal waters containing natural

photosensitizers. Environ. Sci. Technol. 47, 1870–1878. https://doi.org/10.1021/es3036913

Silverman, A.I., Sedlak, D.L., Nelson, K.L., 2019a. Simplified Process to Determine Rate Constants for Sunlight-Mediated Removal of Trace Organic and Microbial Contaminants in Unit Process Open-Water Treatment Wetlands. Environ. Eng. Sci. 36, 43–59. https://doi.org/10.1089/ees.2018.0177

Silverman, A.I., Tay, N., Machairas, N., 2019b. Comparison of biological weighting functions used to model endogenous sunlight inactivation rates of MS2 coliphage. Water Res. 151, 439–446. https://doi.org/10.1016/j.watres.2018.12.015

Sinton, L.W., Hall, C.H., Lynch, P. a, Davies-Colley, R.J., 2002. Sunlight Inactivation of Fecal Indicator Bacteria and Bacteriophages from Waste Stabilization Pond Effluent in Fresh and Saline Waters. Appl. Environ. Microbiol. 68, 1122–1131. https://doi.org/10.1128/AEM.68.3.1122

Sobol', I.M., 1993. Sensitivity analysis for nonlinear mathematical models. Math. Model. Comput. Exp. 1, 407–414. https://doi.org/10.18287/0134-2452-2015-39-4-459-461.

United Nations, 2015. Sustainable Development Goals Knowledge Platform [WWW Document]. URL https://sustainabledevelopment.un.org/sdgs (accessed 4.9.19).

Verbyla, M., von Sperling, M., Maiga, Y., 2017. Waste Stabilization Ponds, in: Rose, J.B., Jiménez-Cisneros, B. (Eds.), Global Water Pathogens Project. Part 4 Management of Rish from Excreta and Wastewater. UNESCO, pp. 1–18.

Verbyla, M.E., Mihelcic, J.R., 2015a. A review of virus removal in wastewater treatment pond systems. Water Res. 71, 107–124. https://doi.org/10.1016/j.watres.2014.12.031

Verbyla, M.E., Mihelcic, J.R., 2015b. A review of virus removal in wastewater treatment pond systems. Water Res. 71, 107–124. https://doi.org/10.1016/j.watres.2014.12.031

Victor, R., Kotter, R., O'Brien, G., Mitropoulos, M., Panayi, G., 2006. Wastewater Use in Agriculture, in: WHO Guidelines for the Safe Use of Wastewater, Excreta and Greywater. World Health Organization, Geneva, pp. 1–196.

von Sperling, M., 2007. Volume 3: Waste Stabilisation Ponds, in: Biological Wastewater Treatment Series. IWA, pp. 1–162.

World Health Organization, 2018. World health statistics 2018: monitoring health for the SDGs, sustainable development goals, World Health Organization. https://doi.org/10.22201/fq.18708404e.2004.3.66178

World Health Organization, 2016. Immunization, Vaccines and Biologicals [WWW Document]. World Heal. Organ. URL https://www.who.int/immunization/monitoring_surveillance/burden/estimates/rotavirus/en/ (accessed 4.9.19).

World Health Organization, 2000. Monitoring Bathing Waters – A Practical Guide to the Design and Implementation of Assessments and Monitoring Programmes, Urban Water. World Health Organization. https://doi.org/10.1016/S1462-0758(02)00006-7

APPENDIX A: INPUTS TO SMARTS IN SIMULATIONS FOR SENSITIVITY ANALYSES

Table 3. Values input to SMARTS for Morris method

Parameter	**Input**	**Unit**
Latitude	Random sampled value	°
Altitude	Random sampled value	km
Height	0.00	km
Atmosphere*	Choose among the reference atmospheres according to location and season	
Water vapor	Calculated from reference atmosphere and altitude	
Columnar ozone abundance	Default from reference atmosphere	
Gaseous absorption and pollution	Default from reference atmosphere	
CO_2	370	ppmv
Extraterrestrial spectrum*	Gueymard 2004	
Aerosol model*	Shettle & Fenn Rural	
Atmospheric turbidity	130 (meteorological range)	km
Regional albedo	Water: water or calm ocean	
Tilted surface and local albedo	Bypass tilt calculations	
spectral range	280-710	nm
Solar constant	1366.1	$W \cdot m^{-2}$
Output variables to print	Global tilted photon flux density	
Circumsolar calculations	Bypass	
Extra scanning/smoothing	Bypass	
Extra illuminance calculations	Bypass	
Extra UV calculations	Bypass	
Longitude	Random sampled value	°
Year	2017	
Month	Random sampled value	
Day	22	
Time zone	Empirical value of the location	

* suggested by SMARTS

Table 4. Values input to SMARTS for Sobol method

Parameter	**Input**	**Unit**
Latitude	Random sampled value from SRTM land area(Jarvis et al., 2008)	°
Altitude	Empirical value of the location in SRTM(Jarvis et al., 2008)	km
Height	0.00	km
Atmosphere*	Choose among the reference atmospheres according to location and season	
Water vapor	Calculated from reference atmosphere and altitude	
Columnar ozone abundance	Default from reference atmosphere	
Gaseous absorption and pollution	Default from reference atmosphere	
CO_2	370	ppmv
Extraterrestrial spectrum*	Gueymard 2004	
Aerosol model*	Shettle & Fenn Rural	
Atmospheric turbidity	130 (meteorological range)	km
Regional albedo	Water: water or calm ocean	
Tilted surface and local albedo	Bypass tilt calculations	
spectral range	280-710	nm
Solar constant	1366.1	$W \cdot m^{-2}$
Output variables to print	Global tilted photon flux density	
Circumsolar calculations	Bypass	
Extra scanning/smoothing	Bypass	
Extra illuminance calculations	Bypass	
Extra UV calculations	Bypass	
Longitude	Random sampled value from SRTM land area(Jarvis et al., 2008)	°
Year	2017	-
Month	Random sampled value	-
Day	22	-
Time zone	Empirical value of the location	-

* suggested by SMARTS

APPENDIX B: ADDITIONAL RESULTS

Table 5. Inactivation rate constants in existing studies.

Citation	Virus	k_{total} [h^{-1}]	k_{endo} [h^{-1}]	k_{exo} [h^{-1}]	Conditions
Mattle et al. (2015)	MS2	0.17 ± 0.01	0.09	0.06	Simulated sunlight; WSP water; depth = 1.6 cm
	PhiX174	0.43 ± 0.07	0.41	0.01	
Kohn et al. (2016)	MS2	[0.149, 0.173]	-	-	Simulated sunlight; WSP water; depth = 1.6 cm
	PhiX174	[0.379, 0.501]	-	-	
Silverman et al. (2015)	MS2	1.4	0.2	1	Treatment wetland water; depth = 5 cm
	MS2	1.3	0.1	0.9	Treatment wetland water; depth = 20 cm
Love et al. (2010)	MS2	0.43 ± 0.02	-	-	Simulated sunlight, Avon Bay sunlight; clear water; filtered seawater
	Adenovirus	0.59 ± 0.04	-	-	
Kohn and Nelson (2007)	MS2	0.72 ± 0.09	-	-	Filtered WSP water, water with Fluka humic acid or Suwannee River humic acid
Silverman et al. (2013)	MS2	[0.2, 0.5]	[0.1, 0.2]	-	Simulated sunlight; coastal water
	Adenovirus	[0.3, 0.8]	[0.1, 0.2]	-	
Nguyen et al. (2014)	MS2	-	0.73 ± 0.03	-	Treatment wetland water; Quartz tube
	MS2	-	0.22 ± 0.01	-	Treatment wetland water; Beaker

Table 6. Results of KS test comparing the empirical parameter distributions of samples that yield two different cases: **1)** $k_{total}^{\text{PhiX174}} \geq k_{total}^{\text{MS2}}$ *and* $k_{total}^{\text{PhiX174}} \geq k_{total}^{\text{adenovirus}}$; **2)** $k_{total}^{\text{PhiX174}} < k_{total}^{\text{MS2}}$ *or* $k_{total}^{\text{PhiX174}} < k_{total}^{\text{adenovirus}}$. Only significantly different distributions are presented.

Parameter	Mean value		$D_{n,m}$
	Case 1 (n = 27,936)	Case 2 (m = 8,064)	($p < 2.2 \times 10^{-16}$)
Zenith angle [°]	53.0	76.5	0.54804
[NPOC] [mg-C·L^{-1}]	19	27	0.31597
Time from noon [h]	2.8	4.0	0.29333
Water depth [m]	1.46	1.80	0.15994
Latitude [°]	29.77	39.38	0.12647

Table 7. Results of KS test comparing the empirical parameter distributions of samples that yield two different cases: **1)** $k_{total}^{\text{adenovirus}} \geq k_{total}^{\text{MS2}}$; **2)** $k_{total}^{\text{adenovirus}} < k_{total}^{\text{MS2}}$. Only significantly different distributions are presented.

Parameter	**Mean value**		$\boldsymbol{D_{n,m}}$
	Case 1 (n = 15,840)	Case 2 (m = 20,160)	($p < 2.2 \times 10^{-16}$)
Zenith angle [°]	46.9	67.1	0.43698
[NPOC] [mg-C·L^{-1}]	15	25	0.33568
Time from noon [h]	2.5	3.7	0.26497
Water depth [m]	1.33	1.69	0.16551
Latitude [°]	27.64	35.28	0.10130

Table 8. Results of KS test comparing the empirical parameter distributions of samples that yield two different cases: **1)** $k_{exo}^{\text{WSP water}} \geq k_{exo}^{\text{natural water}}$; **2)** $k_{exo}^{\text{WSP water}} < k_{exo}^{\text{natural water}}$. Only significantly different distributions are presented.

Parameter	**Virus**	**Mean value**		$\boldsymbol{D_{n,m}}$	$\boldsymbol{p}$
		Case 1 (n)	Case 2 (m)		
[NPOC] [mg-C·L^{-1}]	Adenovirus	22.7 (16,182)	2.1 (1,818)	0.87797	< 2.2×10^{-16}
	MS2	22.3 (16,560)	1.7 (1,440)	0.87886	< 2.2×10^{-16}
	PhiX174	23.5 (15,318)	3.9 (2,682)	0.81443	< 2.2×10^{-16}
[NO_3^-] [10^{-4} M]	MS2	4.87 (16,560)	5.46 (1,440)	0.10348	9.7×10^{-13}

Table 9. Water chemistry parameters of natural water and WSP water in simulations.

Parameter	Natural water	WSP water
[CO_3^{2-}] [M]	4.94×10^{-6}	2×10^{-5}
[HCO_3^-] [M]	1.04×10^{-3}	4.3×10^{-3}
$\Phi_{\cdot OH}^{CDOM}$, unitless	3×10^{-5}	8.09×10^{-5}
$\eta_{CO_3^{\cdot-}}^{CDOM}$ [M^{-1}]	6.5×10^{-3}	1×10^{-2}
$\Phi_{^1O_2}^{CDOM}$, unitless	1.25×10^{-3}	6.63×10^{-3}
$\Phi_{^3CDOM^*}^{CDOM}$, unitless	1.28×10^{-3}	1.1×10^{-2}
$^{\bullet}$OH scavenging rate constant [L·mg-C^{-1}·s^{-1}]	5×10^4	3.176×10^4
$CO_3^{\bullet-}$ scavenging rate constant [L·mg-C^{-1}·s^{-1}]	1×10^2	1.32639×10^5
^{3}CDOM* quenching rate constant [s^{-1}]	5×10^5	3.32×10^6

Table 10. Total effect S_{Ti} of parameters in Sobol analysis

Parameter	Natural water			WSP water		
	Adenovirus	**MS2**	**PhiX174**	**Adenovirus**	**MS2**	**PhiX174**
Month	0.102	0.084	0.104	0.106	0.071	0.108
Time	0.475	0.427	0.479	0.484	0.373	0.484
Location	0.240	0.172	0.245	0.245	0.118	0.249
α	0.001	0.000	0.001	0.004	0.005	0.005
β	0.037	0.018	0.040	0.029	0.083	0.036
[NPOC]	0.224	0.136	0.219	0.172	0.089	0.195
[NO_3^-]	0.002	0.005	0.003	0.003	0.006	0.004
[NO_2^-]	0.003	0.005	0.003	0.004	0.001	0.004
$k_{virus,\cdot OH}$	0.000	0.000	0.000	0.000	0.000	0.000
$k_{virus,CO_3^{\cdot-}}$	0.000	0.001	0.000	0.000	0.001	0.000
$k_{virus,^1O_2}$	0.000	0.024	0.000	0.000	0.168	0.000
$k_{virus,^3CDOM^*}$	0.000	0.013	0.000	0.000	0.006	0.000
Φ_{virus}	0.016	0.027	0.002	0.016	0.008	0.002
ε_{virus}	0.083	0.024	0.089	0.087	0.007	0.093
Water depth	0.749	0.713	0.750	0.731	0.641	0.721

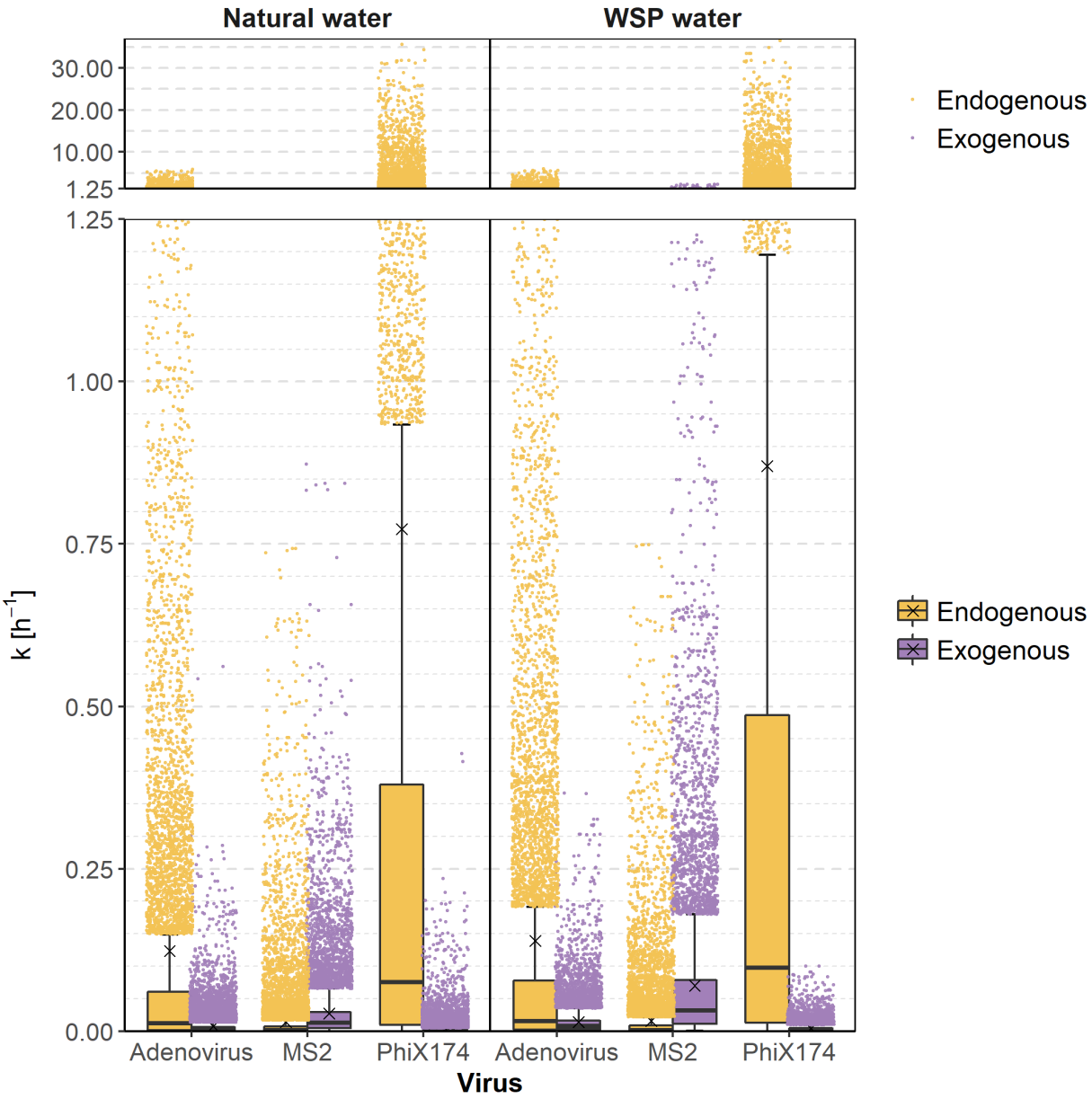

Figure 12. Distributions of modeled endogenous and exogenous inactivation rate constants for Morris analysis. The box indicates 1st, 2nd and 3rd quartiles. The lower whisker shows the minimum, and the upper whisker = q3 + 1.5*IQR. "×" indicates the mean value. Outliers are spread out horizontally for better visualization.

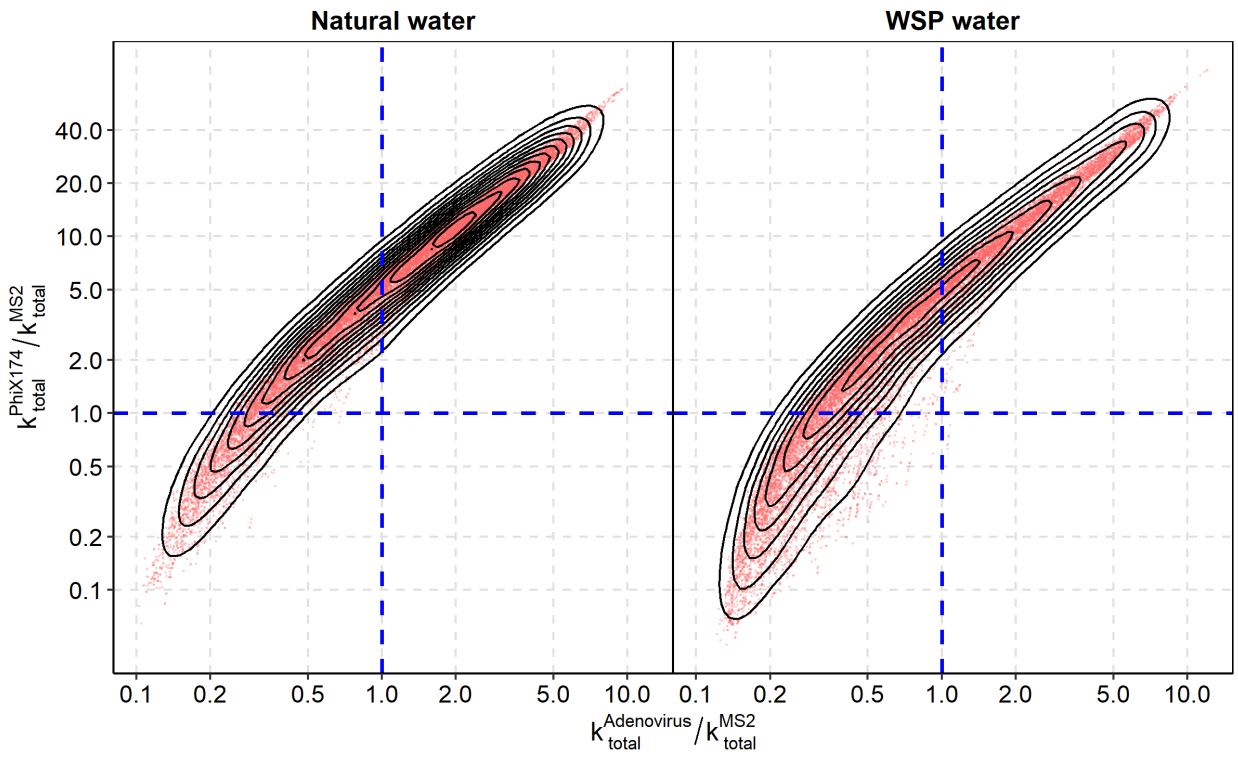

Figure 13. Pair-wise comparison of simulated k_{total} between virus species. Identical sampling matrices were used for all virus-water combination. In consequence, each virus-water combination has the exact same samples for environmental and design parameters. Most of the sample locates above y = 1 and y = x, meaning phiX174 was the most susceptible virus in most cases. About half the sample locates on both sides of x = 1, i.e., adenovirus and MS2 had similar resistance to sunlight inactivation, depending on the environmental, water quality and design parameters.

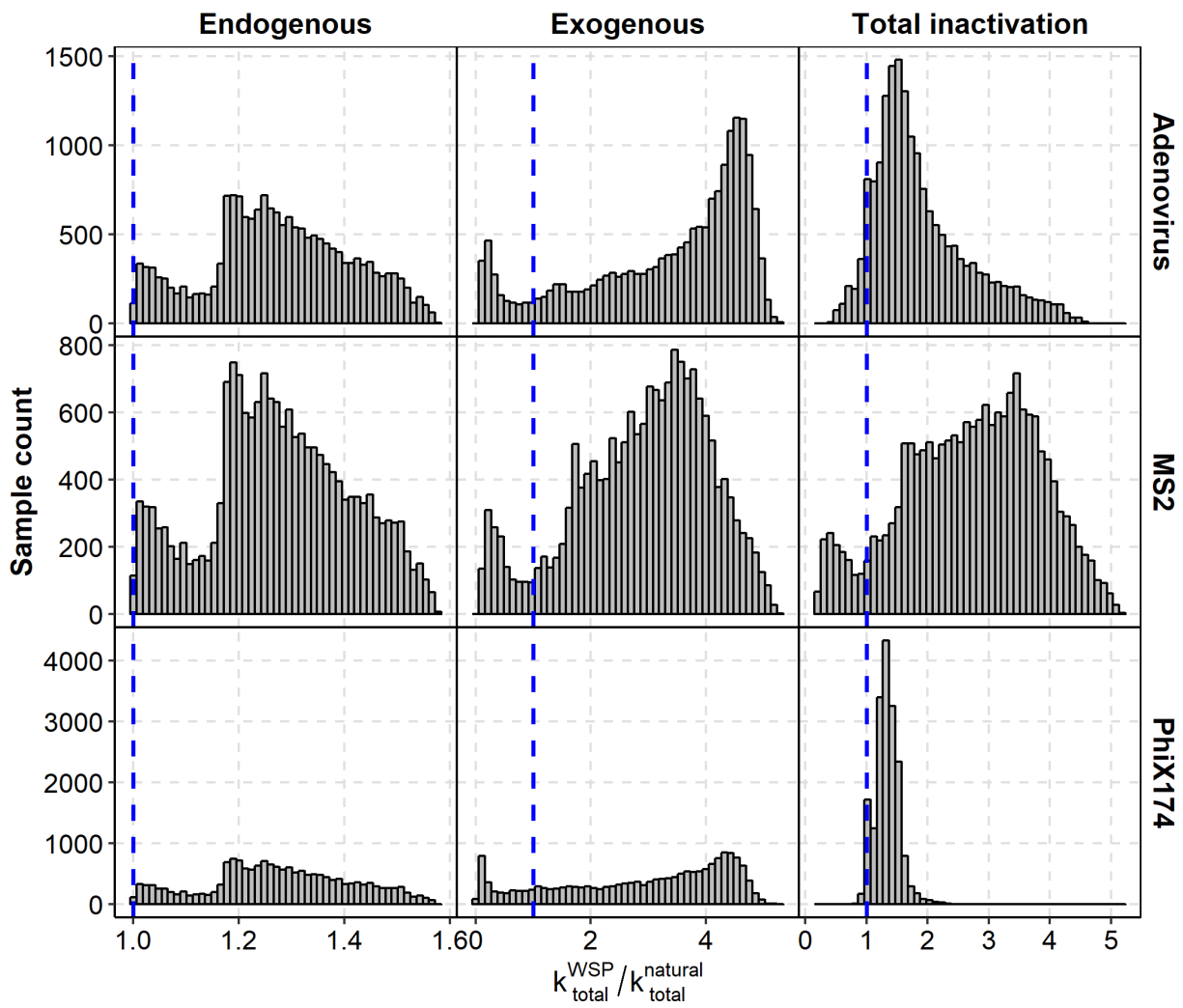

Figure 14. Pair-wise comparison of simulated $k_{total}, k_{endo}, k_{exo}$ between water types. Identical sampling matrices were used for all virus-water combination. In consequence, each virus-water combination has the exact same samples for environmental and design parameters. Regardless of virus species, k_{endo} was larger in WSP water in any case, but k_{exo} was larger in natural water in some cases.

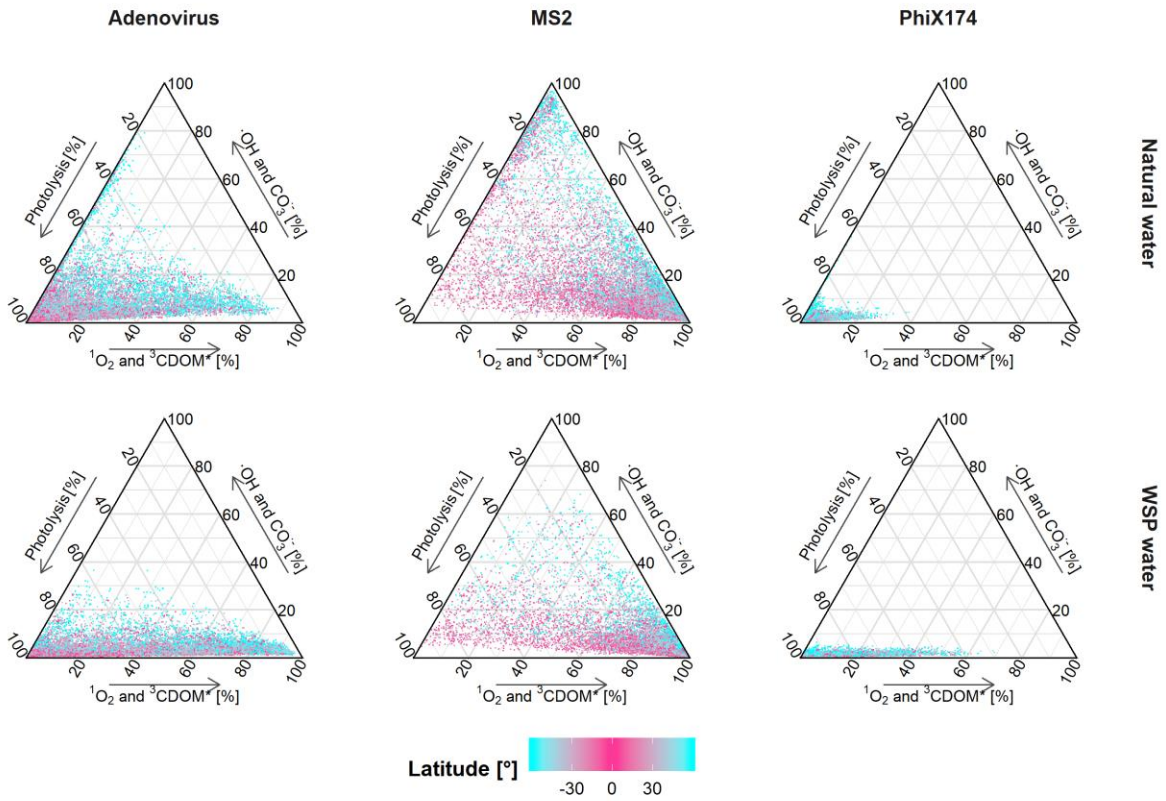

Figure 15. Ternary plot of contributions of inactivation by different mechanisms vs. latitude in simulation. $^3CDOM^*$ and $^1O_2$ were grouped as single-source reactive species. $^\bullet OH$ and $CO_3^{\bullet-}$ were grouped as multiple-source reactive species. The only source of $^3CDOM^*$ was CDOM and the only source of $^1O_2$ was $^3CDOM^*$, while $^\bullet OH$ also had NO_3^- and NO_2^- besides CDOM as sources, and $^\bullet OH$ itself as well as $^3CDOM^*$ were sources of $CO_3^{\bullet-}$.

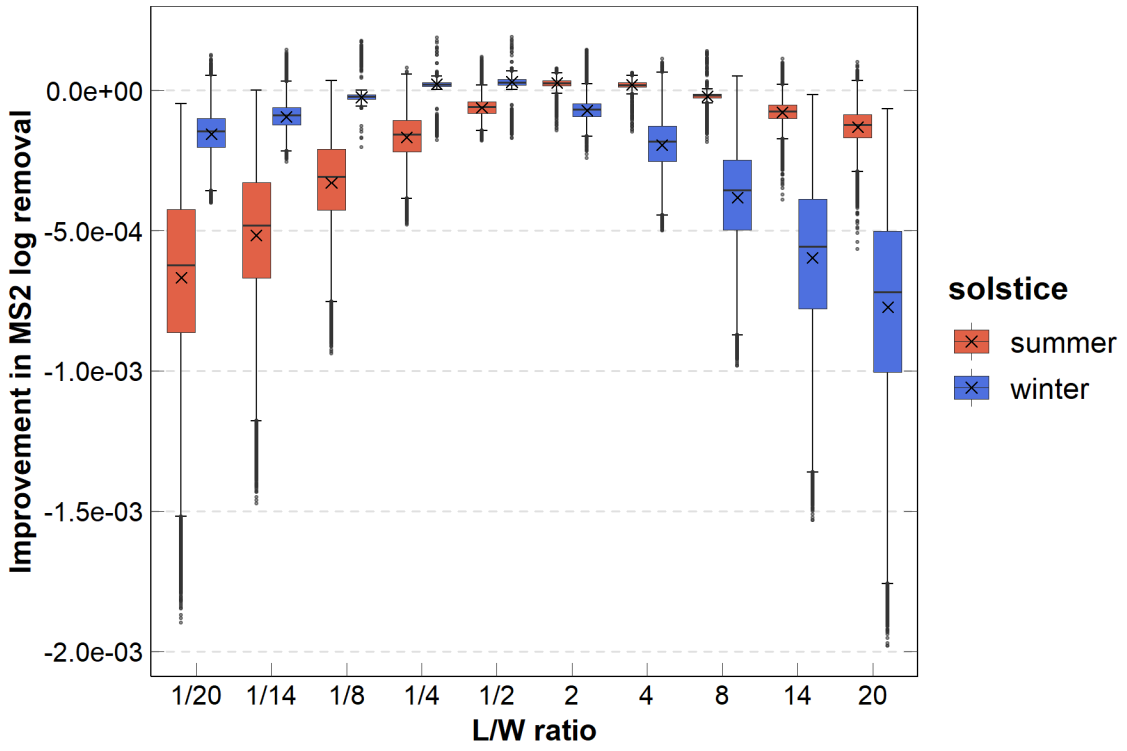

Figure 16. Improvement in MS2 log removal by adjusting L/W ratio from 1. $L/W < 1$ means the short walls are aligned with latitude. MS2 log removal decreases with increasing length-to-width ratio due to blockage of sunlight by pond walls. Long walls facing east-west direction can reduce the negative impact of sunlight blockage on winter time virus removal. However, the reduction of MS2 log removal by changing pond length-to-width ratio or pond orientation are negligible compared to other design parameters.